

CONCORDIA UNIVERSITY

MASTER THESIS

Geometric Simulation and Additive
Manufacturing of Multi-Material Soft
Robots

Author:

Christopher-Denny MATTE

Supervisor:

Dr. Tsz Ho KWOK

*Presented in Partial Fulfillment of the Requirements
for the Degree of Master of Sciences (Mechanical Engineering) at
Concordia University
Montreal, Quebec, Canada*

September 1, 2019

Declaration of Authorship

This is to certify that the thesis prepared

By: Christopher-Denny MATTE

Entitled: Geometric Simulation and Additive Manufacturing of Multi-Material
Soft Robots

and submitted in partial fulfillment of the requirements for the degree of

Ma.Sc Mechanical Engineering

complies with the regulations of the University and meets the accepted standards
with respect to originality and quality.

Signed by the Final Examining Committee:

Dr. Krzysztof Skonieczny Examiner

Dr. Wen-Fang Xie Examiner

Dr. Tsz-Ho Kwok Supervisor

Approved by: _____

Date: September 16th 2019

Dean of Faculty

CONCORDIA UNIVERSITY

Abstract

Gina Cody School of Engineering and Computer Science
Mechanical, Industrial and Aerospace Engineering

Ma.Sc

**Geometric Simulation and Additive Manufacturing of Multi-Material Soft
Robots**

by Christopher-Denny MATTE

Soft Robots have been an increasingly studied topic due to their ability to deal with unknown situations, their inherent compliance which reduces computational load for control by allowing the robot to conform to complex scenarios without requiring precise movement or actuation when compared to rigid robots, as well as the ability to more safely interact with humans. As such a need to simulate soft robots has also developed. Furthermore, the ability to create robots with varying materials allows for designs with additional degrees of freedom as well as pre-programmed deformations. Soft robots can be thought as deforming through geometric constraints; from the shortening of a cable, or the increase in volume of a pneumatic system. A new framework has been developed to simulate multi-material soft robots using geometric modelling. This frame work provided a 45x increase in computational speed compared to commercial software such as Abaqus. In addition, it provides stable and accurate results past 30% strains which current state-of the art solver such as SOFA can not perform. To be able to take full advantage of the design freedom for soft robots, new manufacturing techniques need to be investigated. Conventional manufacturing techniques for elastomers struggle with complex geometry and multi-material fabrication. Additive manufacturing, in certain cases, has been able to address both those issues. While standard Fused Deposition Method and PolyJetting 3D printing techniques are capable of multi-material fabrication, both have inherent flaws that Digital Light Processing 3D printing can address. Therefore a novel multi-material solution was

developed for the DLP process. This printer utilizes an active cleaning solution using a spray to reduce contamination and cleaning time. In addition, an automated storage and retrieval system is adapted to increase the efficiency and material capacity of the printer. When compared to the state of the art, a $3x$ speed increase is observed while having a build area that is 12 times larger, while also decreasing the cleaning time by $8x$ and decreasing contamination by $4x$.

Acknowledgements

I would like to acknowledge everyone who helped me during my degree. Guoxin Fang for his help with the simulation Framework. My capstone team: Felix Trottier-Cournoyer, Michael Pearson and Andrew Dafoe, for their hard work and dedication to making the Multi-Material DLP printer a reality. My parents and friends for their unconditional support. Additionally, I would like to thank both Tom Downey and Chantal Simard for igniting my passion for science during my early education. Finally I would like to thank my supervisor Tsz-Ho Kwok for his mentorship and guidance throughout the process of my Master's, as well as his encouragement to continue my academic career.

Contents

Declaration of Authorship	ii
Abstract	iii
Acknowledgements	v
1 Introduction	1
2 Related Work	6
2.1 Simulation of Soft Robots	6
2.2 Multi-Material 3D Printing	7
2.2.1 Applications	8
2.2.2 Multi-material 3D printing	8
2.2.3 Multi-material SLA/DLP printing	8
3 Geometry-based Direct Simulation for Multi-Material Soft Robots	10
3.1 Introduction	10
3.2 Geometry-based Simulation	11
3.3 Actuation as Geometry Constraints	14
3.3.1 Cable-driven actuation	15
3.3.2 Pneumatic actuation	16
3.4 Shape Parameters for Multiple Materials	16
3.4.1 Deformation with different materials	17
3.4.2 Calibration of shape parameter	19
3.5 Results	20
3.5.1 Comparison with the SoftRobots plug-in for SOFA	21
3.5.2 Verification	21
3.6 Conclusion	21

4	Multi-Material Digital-Light-Processing Printer	24
4.1	Introduction	24
4.2	Material Storage and Retrieval System	25
4.2.1	Storage System	26
4.2.2	Material Swapping	27
4.3	Active Cleaning System	29
4.3.1	Spraying Mechanism	30
4.3.2	Sustainability	31
4.4	Results	32
4.4.1	Material Swapping	34
4.4.2	Cleaning System	36
4.5	Conclusion	38
5	Conclusion	39
A	Local Global Solver	42
A.1	Local projection step	42
A.2	Global assembly step	43
B	Printer Architecture	45
B.1	Printer Base	45
B.1.1	Top level	45
B.1.2	Middle level	45
B.1.3	Bottom level	46
B.2	Build Platform	46
B.3	Material Tower	47
B.4	Material Vats	48
B.5	Electronics and Software	48

List of Figures

1.1	Multi-material applications: A) Physiologically accurate rib cage [1]. B) 3D printed Quantum Dot-LED. Reprinted with permission from [2]. C) A soft robotic hand. Reprinted, with permission, from [3]. D) A conductive Hydrogel and Ecoflex circuit. CC by 4.0 [4].	3
3.1	A cable-driven soft hand with multiple materials. (a) The digital model designed with different material compositions on different fingers. (b) The actuated physical model fabricated by 3D printing, and the fingers have different shapes under the same actuation. (c) The simulation result generated by the proposed method.	11
3.2	(a) A bar is being twisted by 90° . (b) The result without preserving its shape looks unreal. (c) By preserving the original shape of each element, the numerical simulation can mimic the physical phenomenon.	12
3.3	The geometric constraints of actuation. (a) In cable-driven actuation, the gaps are modeled as tetrahedral elements and the edges aligned with the cable will be shortened as the cable is stretched. (b) In pneumatic actuation, the chamber are modeled by tetrahedral elements, which will expand when air is pumped in.	14
3.4	(Top) The target shape for rigid material is computed by rotating the initial shape to align with the current shape. (Bottom) The target shape for extremely soft material is computed by scaling the current shape to preserve the volume of the initial shape. (Right) The shape blending method is applied to align the rigid and the soft materials, and merge their shapes using material property to define the target shape for an intermediate material.	17

3.5	Calibration of the shape parameter for simulating objects with multiple materials: (a) a multi-material bar with displacement on the right, (b) a physical elongation test on 3D printed specimen using NinjaFlex and Flexible PLA materials, (c) a simulation result by using the Abaqus FEA software, (d) the result generated by our simulation framework, and (e) the calibrated relationship between R_m and R_ω	18
3.6	Comparisons on a cable-driven gripper among physical test (left), our simulation(middle), and the simulation by the SoftRobots plug-in for SOFA [5](right).	20
3.7	Two cable-driven soft grippers (left and right) with different material distributions have different behaviors under actuation. Locations of markers determined by our simulation are well-matched with theirs in physical test.	22
3.8	Pneumatic-driven soft gripper: (top) the results of our simulation and (bottom) physical test by increasing the pressure of air pumped into the chamber. The gripper is fabricated by the NinjaFlex material. . .	23
4.1	Material tower with vats and silicone brush	26
4.2	Material swapping process: 1) The material swapping process starts with the cleaning vat pushing the material vat into the tower. 2) The tower lowers to disengage the hooks. 3) The cleaning vat moves back to allow clearance of the hooks, and the tower selects the next material. 4) The material vat advances and the tower rises to engage the hooks. 5) The cleaning vat pulls the material vat into place	28
4.3	Spray pattern of the 3 sprinkler heads	30
4.4	Cleaning system: sprinklers, brush, drain and reservoir	31
4.5	Multi-Material DLP Printer Prototype	33
4.6	Examples of multi-material prints: A) 4 colored die; B) Ball in a cage with two colors; C) Concordia printed in 3 colors on a semi-flexible backing.	34

4.7	Figure shows the breakdown of the varying steps within the material swapping process. In green are the tasks that involve moving and swapping the material vat. In blue are the steps involved in the cleaning process	35
4.8	Pieces used for contamination test. Top left: Four inverted Pyramids . Top Right: Staggered Cone. Bottom Left: Scaffold. Bottom Right: Cylinder	36
B.1	Printer base with detailed components and sectioning	46
B.2	Parallel linear stage with build platform	47
B.3	Custom software depicted during operation	49

List of Tables

4.1	Comparison of previous prototype and ours	34
4.2	Contamination test results, weight in g. U/S = Ultrasound	37

Chapter 1

Introduction

In recent years, soft robotics has become a popular multidisciplinary research area due to its increased robustness and safety compared to traditional robots. Innovations are being made in many fields such as exploration robots, life-like replicas, and the field of bionics. Most common designs for soft robots are realized by distributed actuation on soft materials [6]. With more *Degree-of-Freedom* (DoF) than rigid robots can provide, it can better complete highly dexterous tasks like grasping [7] and detection of confined areas [8]. Soft robots have the unique property that their entire deformation and use case is based on its shape and material distribution. As such being able to program deformations by changing its geometry or placing certain materials in key locations is a very attractive perspective. To fully achieve the potential of soft robots, several areas must be researched. Firstly, since soft robots can have infinite DoF, experience large deformation, and have non-linearities in their control, new methods of simulation need to be investigated to efficiently reproduce them. Additionally the current fabrication methods may be limiting in their ability to create complex geometry with varying material properties.

Due to the high DoF many challenges have arose in numerical simulations. Unlike the rigid robots for which the forward and inverse kinematics can be used to compute the position of an end-effector or the joint parameters, soft robots are deformable continuous objects which can be actuated by various mechanisms. The problem to be solved is how to predict the deformed shape of a soft manipulator fabricated with multiple materials effectively. A common technique for estimating the deformation of elastic materials is the *Finite Element Method* (FEM). However, the FEM methodology relies on the accurate input of structural loads and material properties, which

is not easy to obtain in many scenarios for soft robots. Actually, actuations in soft robotics are often defined by geometric variations. For instance, a cable-driven gripper actuated by motors [9] is controlled by the change in length of cables. Pneumatic actuators are usually driven by the volume change in a chamber [10]. Converting these actuations into structural loads will cause unnecessary errors of approximation. Additionally the relative properties of materials, as opposed to their absolute physical properties, is of a greater interest for soft robots since it will dictate their deformation behavior under these geometric changes. For example, the cable-driven soft hand shown in Fig.1.1(c) is 3D-printed with two materials having different elasticity. The fingers have the same shape but with different material compositions. When applying the same actuation – i.e., the same length of string being shortened, different deformed shapes are presented on the four fingers. In short, designing soft robots by different material compositions can also achieve a variety of behaviors without changing the shape. Differently from FEM, a novel algorithmic approach is developed in this thesis to compute the deformed shape of a soft manipulator directly. This is done by simulating the actuation constraints as elements that are iteratively converged towards. As such, the framework optimization is to minimize the strain energy of all elements based on their specific target shape. This shape can then be tuned to also represent different relative stiffness between materials by defining a weighting scheme between a rigid shape and one that conserves volume. A detailed explanation of the framework is given in Chapter 3.

Manufacturing of soft robots has also come a long way recently. While molding techniques are used to fabricate soft robots in the past, the advancement in 3D printing allows the fabrication of soft robots with multiple materials [11, 12]. Currently, the world of 3D printing is advancing at great speeds. From increases in performance, accuracy and strength, all the way to the utilization of multiple materials for a single print [13]. Multi-material 3D printing offers designers more DoF in design with fewer limitations allowing them to put more focus on the intended functionality of a product. With more DoF, products can be smarter and can better complete highly dexterous tasks. Some examples of multi-material 3D printed applications are demonstrated in Fig.1.1.

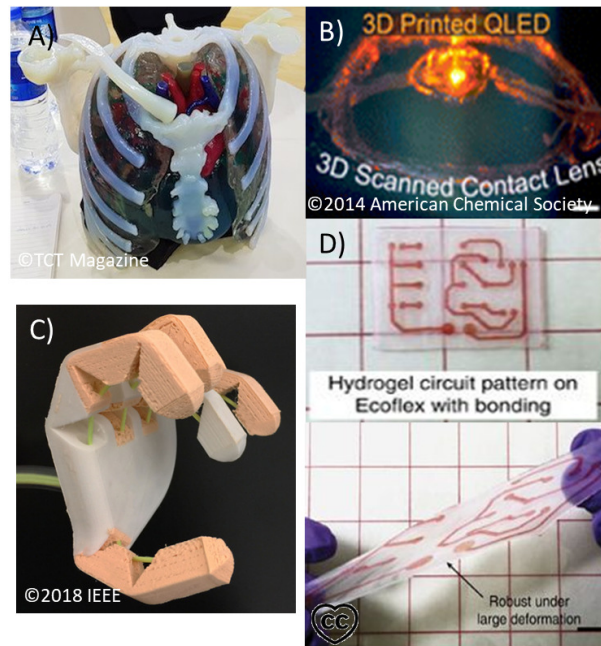


FIGURE 1.1: Multi-material applications: A) Physiologically accurate rib cage [1]. B) 3D printed Quantum Dot-LED. Reprinted with permission from [2]. C) A soft robotic hand. Reprinted, with permission, from [3]. D) A conductive Hydrogel and Ecoflex circuit. CC by 4.0 [4].

There are several existing 3D printing methodologies and each has its own advantages and challenges. Multi-material printing, as a more complex process, adds a unique set of problems to be solved for each of the different methods. Fused deposition modeling (FDM) uses thermoplastics just beyond their melting point and extrudes them, by means of a nozzle, to construct the layers [14]. The polyjetting technique jets the material out of a nozzle similar to FDM, except the material is a photo-curable polymer and is cured using ultraviolet (UV) light as soon as it leaves the nozzle [15]. Due to their deposition mechanisms, both technologies have been able to utilize multiple materials for some time by using multiple nozzles or swapping the feed-stock material. Nevertheless, because of the deposition method, there are also some undesirable characteristics, such as poor coalescence, limited feature size, precision, and anisotropic material properties. In addition, both technologies are limited by the viscous dynamics of their materials through the delivery system of the nozzle. All these characteristics also affect their ability to print flexible materials required for soft robots. Poor coalescence will mean poor performance at large deformations; while the requirement of FDM printers to feed material into a nozzle to force material out limits the flexibility and print-ability of materials.

On the other hand, the stereolithography (SLA) process is one of the most important 3D printing technologies, and also the first one to be commercialized in 1980s. The Digital Light Processing (DLP) process, a variant of SLA, shares the same principle to cure liquid resin to solid through a vat polymerization technique. The main difference is the curing method. While SLA uses a guided laser which cures by drawing out the image layer, DLP cures the entire layer using the projection of an image [16]. However, SLA/DLP printers are still very limited in multi-material printing with only a few researches exploring this technology [17–19]. This is because SLA/DLP printers need to swap entire vats to change materials, which takes far longer than the deposition approaches. Furthermore, whenever there is a swap of material, the part has to be cleaned due to it being submerged in different resins, contaminating both the current layer and previous layers. One way to address this issue is to soak the part in a cleaning solution [18], however it takes a long time to reduce the contamination. In spite of the difficulties, compared to other polymer 3D printing technologies, SLA/DLP produces parts with the highest accuracy and the best surface finish. As such SLA/DLP printing shows itself to be one of the most promising technologies for the future of additive manufacturing. Moreover, as DLP has the ability to print an entire layer at once, its fabrication speed is remarkable. Therefore, there is a huge interest in developing multi-material DLP printing. For these reasons and others a novel multi-material Digital-Light-Processing (DLP) 3D printer utilizing automated storage and retrieval system (ASRS) with an active cleaning approach has been designed. This thesis aims to solve some of the issues with multi-material DLP printing such as contamination between materials by using an active spraying method. It also proposes addressing the challenge of long material swap time, and limited material capability by emulating an ASRS.

The rest thesis will be broken down into 3 main sections. Chapter 2 will go over works related to soft robots, their simulation, and their fabrication using multi-material 3D printers. Chapter 3 will discuss the geometric framework for the simulation of soft robots. While Chapter 4 pertains to the research performed for the novel design of an automated storage and active cleaning multi-material Digital-Light-Processing 3D Printer. Each chapter is broken down further into their respective subsections outlining their contributions, methodologies and implementations. Chapter 5

will summarize and elaborate on the future of these works.

Chapter 2

Related Work

2.1 Simulation of Soft Robots

With a good understanding of material properties and the mechanism of actuation, precise FEA can be conducted with given forces / torques. Commercial software like Abaqus and ComSol have been used in the research of soft robotics [10]. On one hand, small time-steps are needed for systems with large stiffness for simulating large deformation; on the other, it requires modeling complicated multi-material properties as well as their interaction. Additionally when soft robots and actuators get more complicated, inputs for deformation will get more difficult to place and properly deform.

In order to get a fast simulation for interactive and iterative design of soft robots, Hiller and Lipson [20] developed a platform called Voxelyze that is able to generate results of dynamic simulation for multi-material soft objects. Voxel representation is used for simulating large deformation and evolutionary computation is employed to obtain optimized material distributions [21]. Nevertheless, large quantity of voxels are needed to represent models with complex shape, which will tremendously slow down the computation.

SOFA [22] is a widely used framework in the field of surgical and biomedical simulation. This framework proposed a novel method of sectioning models and elements in a scene to increase the efficiency of the solver. They were able to have 3 different models for each object, a physical FEM model, a collision model, and a visual model. By doing so, they can individually optimize the mesh and algorithms for each use case, allowing for a coarse mechanical mesh while maintaining a detailed visual mesh.

Based on SOFA, Duriez *et al.* [5] developed a plug-in for real-time simulation of soft robots that supports interactive deformation. Inverse design can also be conducted by an optimization based algorithm. Their algorithm uses the iterative method to solve ordinary differential equations meanwhile transferring the boundary conditions using Lagrangian multipliers. This method is fast but suffers from the problem of numerical accuracy, particularly if there is large deformation (rotations). They also have a strategy which allows to identify regions of interest to be more detailed and physically simulated while other areas are simple and not considered. This results in a faster and more efficient approach to simulation of soft robots than conventional FEA, but relies on the simplification of the mechanics and the objects to adjust the performance to the users preference. However, one benefit of soft actuator is its capability of adapting to highly curved contact by large deformation [23], which needs to be precisely simulated for many applications. With the help of mass-spring system, Allison *et al.* [24] presented a close-loop control for haptic jamming deformable surface. However, they are application-specific and may not be generalized to other soft actuators.

There is research [25–27] that applies geometry-based algorithm in optimization. Different from using constrained nonlinear optimization [28], the geometry-based numerical computation can converge in a few iterations. This is a novel approach that can be used to more intuitively actuate and simulate soft robots, while decreasing computational load and maintaining mesh quality. Although the basis of this approach has been validated in terms of simple mechanics [29], there is still research to be done about the extents this approach can reach in terms of properly emulating all features classical FEM can perform. This thesis extends this idea to the simulation for soft robots with multiple materials.

2.2 Multi-Material 3D Printing

This thesis is related to multi-material 3D printing, and particularly multi-material SLA/DLP printing. Before reviewing those works, the applications are briefed.

2.2.1 Applications

Multi-material printing allows for the creation of functionally graded materials which have variations in the properties as the dimension varies [30–32]. Utilizing this principle, biopolymer structures and liver cells for free-form construction of 3D tissue scaffolds is possible [33]. In this context the use of multiple materials has allowed for advances in soft robotics by allowing the placement of soft materials with harder materials [34] and the ability to add specific properties such as conductivity to materials and parts [35]. In the field of robotics, more and more design for anthropomorphic hands are utilizing some form of 3D printing with multiple materials. This allows for unique compliance and performance of joints and actuators to better control and design such hands [36–38]. As suggested by Wang et al. [39], the possibilities do not simply extend to the engineering world, artists and fashion designers can also take advantage. From prototypes to end products, it can be seen that the technology is being applied to various fields, from organs to airplane parts [40].

2.2.2 Multi-material 3D printing

Development on multi-material printing is happening for almost all methodologies. For FDM to change materials, it must have multiple nozzles or swap the filaments. This requires motors to pull out and insert the next filament which then must purge the old material left in the model. An example of this is the Prusa i3 multi-material printer [41] as a commercial solution, but the likes of Khalil et al [33] have developed triple extruder system for the printing of scaffolds. Similarly, Leu et al [42] also developed a triple extruder which can control paste extrusion. A multi-material Polyjet printer was created by MIT CSAIL [15] capable of handling up to 15 materials through ink-jetting technology. Selective laser sintering or melting (SLS/SLM) is also a technology that can fabricate multi-material parts by using different powders [43,44].

2.2.3 Multi-material SLA/DLP printing

SLA/DLP technology requires more considerations, as FDM or Polyjet printers would use independent nozzles for various materials, entire resin vats must be used for

SLA/DLP. There are only a few multi-material SLA/DLP printers presented in literature. Holtrup [45] recently constructed a multi-resin DLP printer that has a series of reservoirs arranged linearly between the printing stage. The materials are swapped by engaging a conveyor in order to change the current vat. However, this system has long wait time during cleaning of resin and material swapping. In contrast, a carousel design has been approached and improved upon several times over the last decade. Wicker et al. [46] modified an existing 3D Systems SLA 250/50 and added multi-material capabilities by appending a horizontal carousel to the side of the printer. Inamdar et al. [17] developed a similar system as a standalone solution to multi-material SLA. Like the previous two carousels, Zhou et al. [18] developed another rotary printer, which rotates two material vats along with their cleaning system comprised of brushes and an ultrasonic bath. Alongside these designs is again a rotary design [47] using UV and IR radiation. Though quicker than the linear setup, the rotational printer makes it difficult to increase the number of materials, or the build area as the size of the printer would grow exponentially. The previous works have proved that SLA/DLP technique can be extended to multi-material printing, although with certain challenges still needing to be solved. In this paper, the concept of a storage system is applied to facilitate the material swapping process, and it is presented in the Section 4.2.

Chapter 3

Geometry-based Direct Simulation for Multi-Material Soft Robots

3.1 Introduction

Based on the observation that many actuations in soft robotics are directly related to geometry, it was hypothesized that a geometry-based simulation would give better convergence and accuracy than the standard FEM methods. Here higher accuracy means that the results of simulation are closer to the physical tests. In addition, the simulation should be able to handle multiple materials. To test this hypothesis, techniques from geometric computing are applied to formulate a framework that can directly model and simulate soft robots based on geometry.

To realize the framework, three research questions need to be investigated: 1) How to convert the mechanical analysis to a geometric problem, 2) How to apply different actuations in the simulation, and 3) How to model the material properties geometrically. Answering these questions brings the contributions of this thesis as follows:

1. A geometric optimization to minimize the elastic energy with reference to shape variations is formulated to mimic the physical phenomenon during deformation.
2. The geometric constraints of actuations are modeled by a type of element, which can be directly integrated in the optimization.

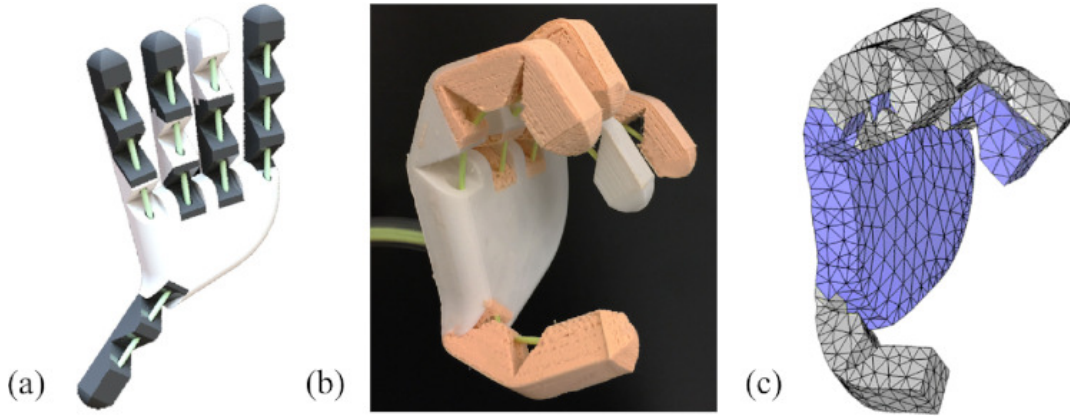


FIGURE 3.1: A cable-driven soft hand with multiple materials. (a) The digital model designed with different material compositions on different fingers. (b) The actuated physical model fabricated by 3D printing, and the fingers have different shapes under the same actuation. (c) The simulation result generated by the proposed method.

3. A simple calibration method is developed to learn the relationship between material properties and shape parameters, which are used in our framework to simulate the deformation of objects with multiple materials.

The framework is direct and efficient, and its functionality will be demonstrated and verified on cable-driven and pneumatic soft robots with multiple materials.

The rest of this chapter is organized as follows. Section 3.2 introduces the framework of the geometry-based simulations. After that, Section 3.3 discusses how to formulate the actuations as geometric constraints, which is followed by presenting a calibration method for multi-material simulation in Section 3.4. The experimental tests and validation are given in Section 3.5, and ends with the conclusion and discussion in Section 3.6 for the framework.

3.2 Geometry-based Simulation

When different boundary conditions or external loads are applied to deform an object \mathcal{M} , the elastic energy is transferred by the corresponding work and distributed internally in the materials of \mathcal{M} . Here the elastic energy is caused by shape deformation, which can be evaluated from the strains (i.e., local deformations throughout \mathcal{M}). In this sense, the total elastic energy can be minimized when the original shape of \mathcal{M} is preserved as much as possible.

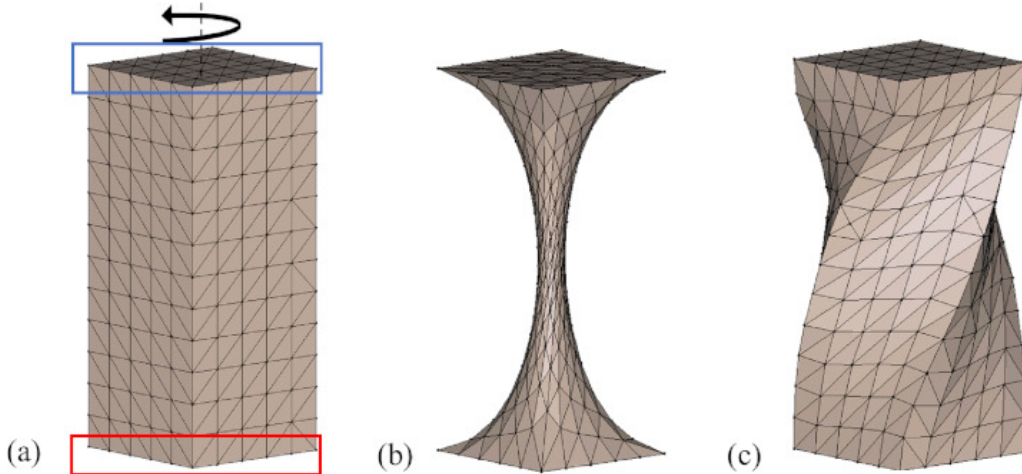


FIGURE 3.2: (a) A bar is being twisted by 90° . (b) The result without preserving its shape looks unreal. (c) By preserving the original shape of each element, the numerical simulation can mimic the physical phenomenon.

$$ElasticEnergy = 1/2 * K * \delta X^2 \quad (3.1)$$

From equation 3.1 it can be seen that the difference in position for a node is an exponential increase in energy, thus having all nodes equally close to their desired position will lead to a minimized global energy. Choa *et al.* [29] modelled this elasticity as the difference between the the differential of a deformation and the rotation group. To mimic this physical phenomenon, this section formulates a geometry-based simulation as an optimization problem to preserve a target shape while satisfying the imposed boundary conditions and actuation constraints as an energy minimization.

Assume a soft robot is digitally represented by a volumetric mesh $\mathcal{M}_s = (\mathcal{V}, \mathcal{E})$, where \mathcal{V} and \mathcal{E} stand for the sets of vertices and elements on the mesh. The shape of the i -th element is defined as $\mathbf{V}_i = [\mathbf{v}_1 \ \mathbf{v}_2 \ \dots \ \mathbf{v}_n]$, where n is the number of vertices of the element, e.g., $n = 4$ for a tetrahedron in this case. Let $\mathbf{V}_i^t = [\mathbf{v}_1^t \ \mathbf{v}_2^t \ \dots \ \mathbf{v}_n^t]$ be the target shape that the element would preserve, then the optimization can be formulated as minimizing the difference between \mathbf{V}_i and \mathbf{V}_i^t for all m elements. That is defined by an energy as

$$E = \sum_{i=1}^m d(\mathbf{V}_i, \mathbf{V}_i^t). \quad (3.2)$$

To measure the difference $d(\cdot, \cdot)$ of two shapes, they have to be properly aligned in terms of both position and orientation. Therefore, both the shapes get centered at

the origin and a rotation is applied to match \mathbf{V}_i^t with \mathbf{V}_i , such that the Equation 3.2 can be further defined as:

$$E = \sum_{i=1}^m \omega_i \|\mathbf{N}\mathbf{V}_i - \mathbf{R}_i(\mathbf{N}\mathbf{V}_i^t)\|_F^2. \quad (3.3)$$

Where ω_i is a weight for each element; normally set as the element's volume. $\|\cdot\|_F$ is the Frobenius norm, and \mathbf{N} is a 4×4 matrix to transfer an element's center to the origin:

$$\mathbf{N}(i, j) = \begin{cases} 3/4 & \text{if } i = j \\ -1/4 & \text{if } i \neq j \end{cases} \quad \forall i, j \in (1, 2, 3, 4).$$

There are two sets of unknowns in Eq.(3.3): one is the positions of vertices \mathbf{V}_i , and the other is the rotation matrices \mathbf{R}_i . The R matrix here is similar to the deformation gradient calculated in standard FEA to compute internal stresses and strains for the element. They are dependent on each other, which leads to a nonlinear system. A two-step iterative method [27] is conducted to solve this problem. Specifically, one set of unknowns is fixed while solving the other set, and the fixed set is switched alternatively between two neighboring steps. This two-step method has been proven to be very efficient [25]. When the target shape \mathbf{V}_i^t for each element has been defined, this framework of optimization can deform the element shape \mathbf{V}_i to approach its target shape as much as possible. Appendix A goes into detail for the process, and highlights the similarity between standard methods and the new geometry approach. The difference in shape locally can be thought as the strain energy of an element, while the global step can be seen as a minimizing of the meshes total strain energy while maintaining continuity, compatibility and obeying the constraints placed on the model.

A demonstration of its functionality is given in Fig.3.2, where a bar in (a) is twisted by 90° (b) without and (c) with preserving the target shapes \mathbf{V}_i^t . The target shape of each element in this example is set as its original shape shown in (a). When applying this optimization based deformation framework for the simulation of soft robots, the problem of defining an appropriate target shape needs to be addressed so that different actuations and materials can be incorporated. These will be discussed in the following sections.

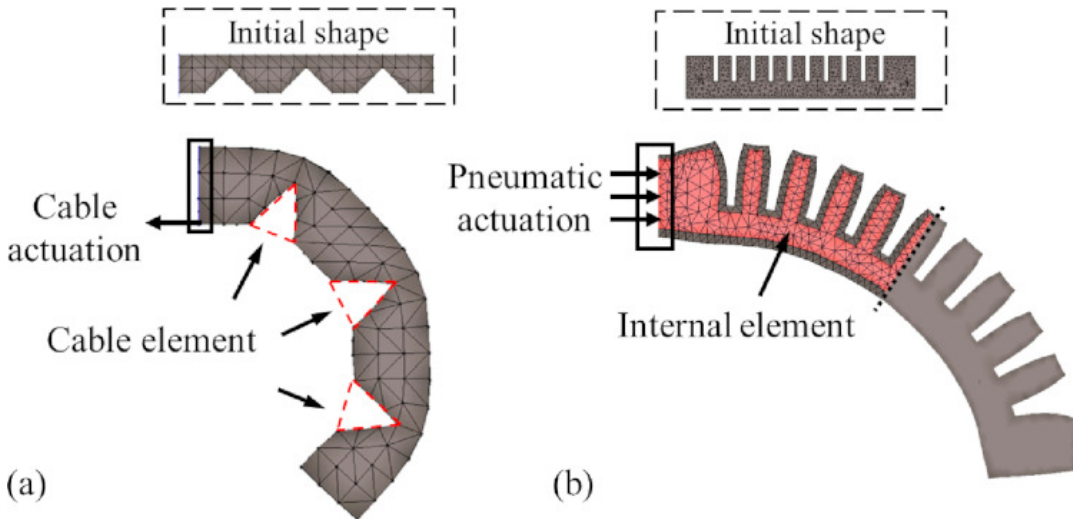


FIGURE 3.3: The geometric constraints of actuation. (a) In cable-driven actuation, the gaps are modeled as tetrahedral elements and the edges aligned with the cable will be shortened as the cable is stretched. (b) In pneumatic actuation, the chamber are modeled by tetrahedral elements, which will expand when air is pumped in.

3.3 Actuation as Geometry Constraints

Soft robots are deformed by external actuations such as shortening the length of a cable or expanding the interior volume of a chamber. These actuations are treated as the geometric hard constraints \mathcal{C} for the simulation framework, which leads to a constrained optimization problem as

$$\min_{\mathcal{V}, \mathcal{R}} E \quad \text{subject to } \mathcal{C}. \quad (3.4)$$

When solving such a problem by a penalty-based method such as the Lagrange multiplier a convergence problem may occur, especially when the initial value is not feasible (i.e., the constraints \mathcal{C} are not satisfied at the initial value of numerical computation). To solve this problem efficiently, the actuation is formulated as a special type of element and uses the target shape \mathbf{V}_i^t to model these hard constraints, which can then be seamlessly integrated to the geometry-based simulation framework. Details about how to convert physical actuations into target shapes for both the cable-driven and the pneumatic actuations are presented below.

3.3.1 Cable-driven actuation

Figure 3.3(a) demonstrates a common model of cable-driven soft gripper, which is a rectangular bar with gaps located in one side. The gripper is fixed at one end, and a cable shown as a dotted line is passed through the holes along the gripper. The gripper is actuated by pulling the cable (i.e., by changing its length). As a result, it bends towards the side with gaps. To integrate the cable in the simulation, the V-shaped gaps are modeled as a set of tetrahedral elements $\tilde{\mathbf{V}}_1, \tilde{\mathbf{V}}_2, \dots, \tilde{\mathbf{V}}_n$.

There is a triangular face on each of these elements that aligns with the cable. These faces called *cable-component* will be used to drive the simulation. The total length of the cable L equals to the length of the gripper that includes the rigid portions R_d and the gaps l_i , i.e., $L = R_d + \sum_{i=1}^k l_i$, where k is the number of gaps. Given the cable-driven actuation with a shrinking ratio S , the geometric constraint is defined as:

$$C_c(\tilde{\mathbf{V}}_1, \tilde{\mathbf{V}}_2, \dots, \tilde{\mathbf{V}}_n) : SL = R_d + \sum_{i=1}^k sl_i, \quad (3.5)$$

where s is a local shrinking ratio for the gaps. If the local shrinking ratio s of a gap is given, the target shape for its corresponding tetrahedral elements can be computed. By rotating the tetrahedral element $\tilde{\mathbf{V}}_i$ to its local coordinate system (resulting in $\tilde{\mathbf{V}}_i^L$) where its cable-component is aligned to the xy -plane, and the main axis of the gap is aligned to the y -axis, the target shape $\tilde{\mathbf{V}}_i^t$ can be computed by scaling in the x -axis, i.e., $\tilde{\mathbf{V}}_i^t = [s \ 1 \ 1] \tilde{\mathbf{V}}_i^L$.

Note that, the input shrinking ratio S is different from the local shrinking ratio s . The problem here is to compute the local shrinking ratio s to satisfy the hard constraint C_c . Computing the ratio and the shapes at the same time is non-linearly coupled and therefore hard to solve. Fortunately, the deformation is a dynamic process with a number of time steps. Therefore the ratio can be determined during optimization. Due to the material distribution, the gaps will be optimized to different shapes. Specifically, starting from $s = 0$, a small shrinking ratio, e.g., 0.01, is added to s for each incremental step in the time domain. This process is iterated until the constraint C_c is satisfied. Figure 3.3(a) shows the simulation result for a shrinking ratio $S = 0.7$.

3.3.2 Pneumatic actuation

A pneumatic actuator usually drives soft robots by pumping pressurized air into a bellow formed by soft materials. As shown in Fig.3.3(b), our method is demonstrated by a commonly used tooth-shape soft gripper. The left part is fixed while air is pumped along the direction of the arrows into the bellows. The internal tetrahedral elements $\tilde{\mathbf{V}}_1, \tilde{\mathbf{V}}_2, \dots, \tilde{\mathbf{V}}_n$ highlighted in Fig.3.3(b) are used to model the expanding behavior of air inside the bellows.

Let the volume of an element be u_i for the i -th element, the total volume of a bellows is then $U = \sum_{i=1}^n u_i$. Given the volume change, the geometric constraint for a pneumatic actuator can be described by an expansion ratio E :

$$C_p(\tilde{\mathbf{V}}_1, \tilde{\mathbf{V}}_2, \dots, \tilde{\mathbf{V}}_n) : EU = \sum_{i=1}^n eu_i \quad (3.6)$$

where e is a local expansion ratio of the internal elements. When e is defined, the target shape $\tilde{\mathbf{V}}_i^t$ for the tetrahedral element can be computed by $\mathbf{V}_i^t = e\tilde{\mathbf{V}}_i^L$ after centering the tetrahedron $\tilde{\mathbf{V}}_i$ to origin.

The process of calculating the final shape of a pneumatic actuator is similar to the cable-driven actuation discussed above, which is to add a small expansion ratio to the elements in each time step and iterate until the constraint C_p is satisfied. Fig.3.3(b) shows the simulation result with given expansion ratio $E = 1.25$.

3.4 Shape Parameters for Multiple Materials

Under an external load, the material deforms and stores potential elastic energy. The total energy can be minimized by preserving the original shape of an object. However, if an object contains multiple materials, regions with different materials will deform in different proportions. In this section, a method is proposed to simulate soft objects with multiple materials by using shape parameters. The relationship between material properties and shape parameters first needs to be found. One can calibrate the relationship by applying the same force to different materials and measuring how much they deform – e.g., a conventional tensile test. However, when the actuation is geometry-based, this calibration is indirect and requires an additional conversion

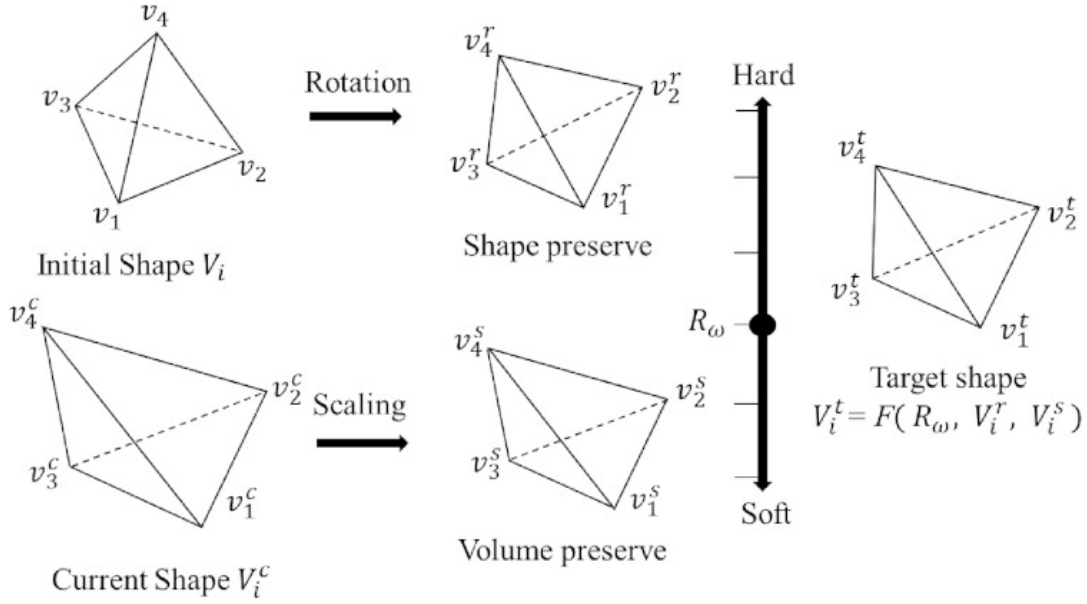


FIGURE 3.4: (Top) The target shape for rigid material is computed by rotating the initial shape to align with the current shape. (Bottom) The target shape for extremely soft material is computed by scaling the current shape to preserve the volume of the initial shape. (Right) The shape blending method is applied to align the rigid and the soft materials, and merge their shapes using material property to define the target shape for an intermediate material.

between force and deformation. Rather than calibrating each material separately with force, a simple method is developed to calibrate the relative properties between two materials. Before that, the method used to model different material properties geometrically is presented.

3.4.1 Deformation with different materials

To model the different properties of materials, a simple way is to assign different weights ω_i for each element in Eq.(3.3), and the shapes of elements with different weights will be preserved differently through the optimization. This mimics the deformation of multiple materials. However, this way of handling the material difference at the global blending step by least-square solution may lead to large approximation error. In order to gain a better control and reinforce the physical property in large deformations, the deformation behavior of elements is controlled at the local step by altering their target shapes, \mathbf{V}_i^t , according to different material properties. Basically, if a material is extremely hard, it will be rigid during the deformation. Respectively, an extremely soft material will deform and conform to its neighbors and external

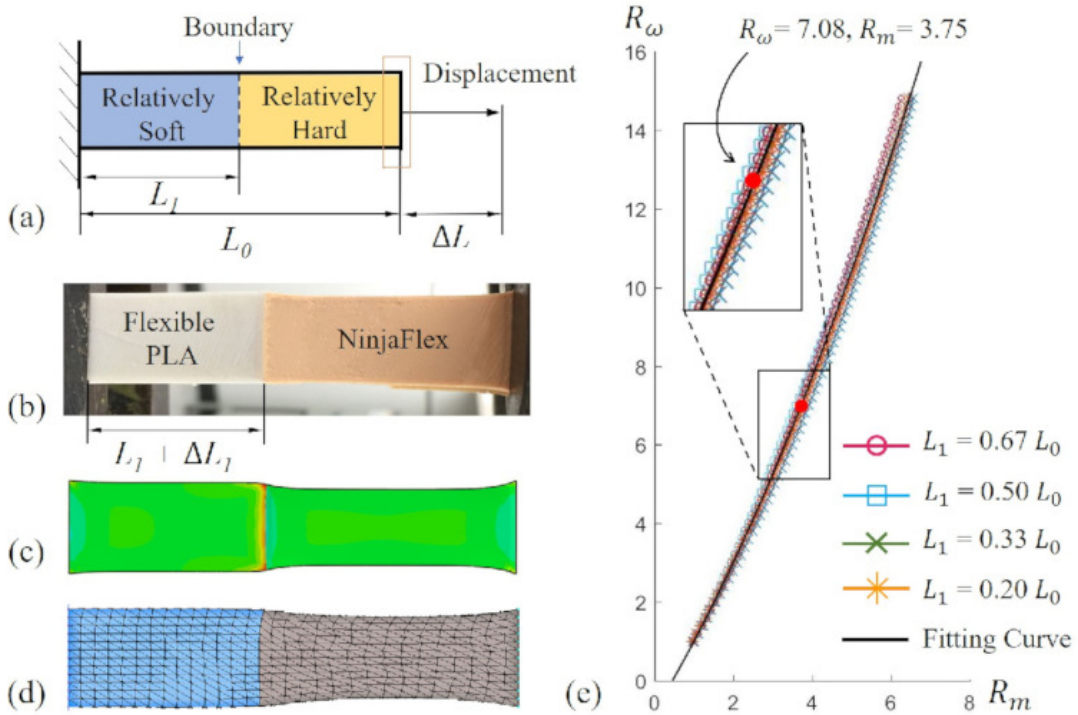


FIGURE 3.5: Calibration of the shape parameter for simulating objects with multiple materials: (a) a multi-material bar with displacement on the right, (b) a physical elongation test on 3D printed specimen using NinjaFlex and Flexible PLA materials, (c) a simulation result by using the Abaqus FEA software, (d) the result generated by our simulation framework, and (e) the calibrated relationship between R_m and R_ω .

constraints while preserving its volume.

A shape blending method is developed in for the framework to compute the target shapes \mathbf{V}_i^t for different materials based on their relative properties. As shown in Fig.3.4, the target shape of a rigid element comes from the rigid transformation of its original shape. For a soft element, its target shape comes from the current shape by scaling back to its original volume (see Fig.3.4). For a material in-between (e.g., with a ratio R_ω), the rigid and soft target shapes are aligned and blended together using the concept of isometric morphing [48] to get the target shape as shown in the right of Fig.3.4.

In this way, the target shapes of elements according to different materials are properly controlled during the deformation, and thus the result of optimization will not be prone to large approximation error caused by least-square solution. The next sub-section will discuss how to determine the ratio R_ω – the shape parameter – for the relative material properties.

3.4.2 Calibration of shape parameter

To calibrate the shape parameter R_ω for the deformation of multiple materials, a displacement is imposed on a rectangular specimen at one end while fixing the other end (as shown in Fig.3.5(a)). Without loss of generality, the specimen is fabricated with two materials A and B joined with a sharp interface. Let the length of the whole specimen be L and the distance between the interface and the fixed end be L_1 , where different values of $L_1 \in (0, L)$ are used for different specimens. When imposing a displacement ΔL at the free end of the bar, the displacement of the interface will be located at $\Delta L_1 \in (0, \Delta L)$ depending on the relative material properties between A and B. The relationship of two materials can be presented by a *material ratio* R_m , which is mathematically defined as

$$R_m = \frac{E_A}{E_B} = \frac{L_1(\Delta L - \Delta L_1)}{(L - L_1)\Delta L_1}, \quad (3.7)$$

where E_A and E_B are the Young's modulus of two materials with A being linked to the fixed end and B locating at the free end. To verify the quality of 3D printed specimens, elongation test are performed on them. The results of physical tests match well with the simulation results generated in Abaqus (see Fig.3.5(b) and (c)).

With this insight, the rest of the problem is to find the relationship between the material ratio R_m and the shape parameter R_ω . The basic idea is to apply different values of R_ω to run the elongation tests in our geometry-based simulation by the same setup (see Fig.3.5(d)). By matching our simulation results with the results of Abaqus, the value of shape parameter R_ω for two particular materials can be determined.

To calibrate the relationship for different material ratios R_m , different values of R_m are applied in Abaqus, which allows to find the matching value of R_ω in the geometric simulator, which is plotted in Fig.3.5(e). Note that samples are also generated by using different values of L_1 (i.e., the locations of the interface) to validate the correctness of calibration. Figure 3.5(e) shows that the data have a very good alignment, and a second order polynomial curve is fitted to define the relationship as

$$R_\omega = 0.114R_m^2 + 1.665R_m - 0.766 \quad (3.8)$$

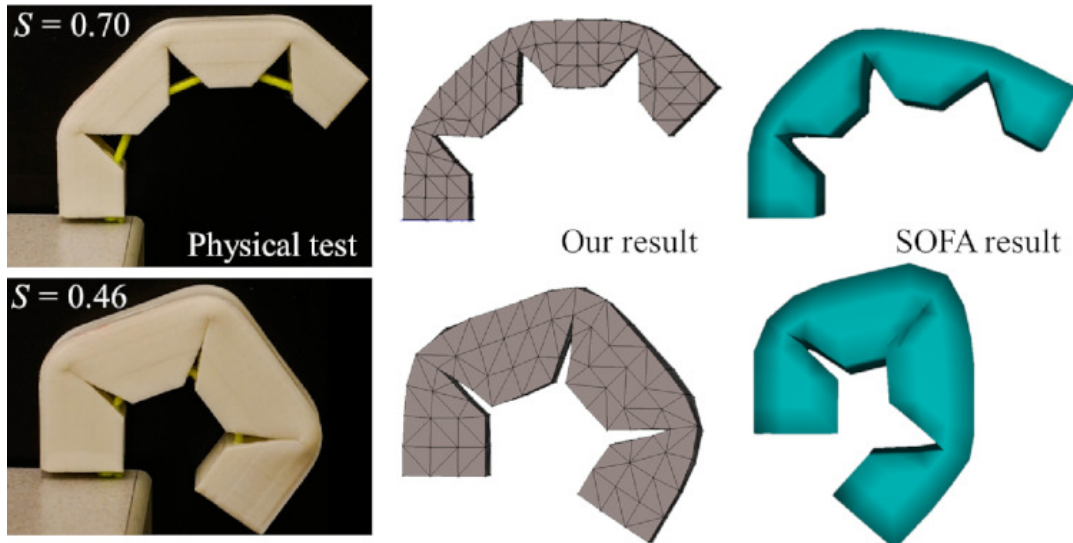


FIGURE 3.6: Comparisons on a cable-driven gripper among physical test (left), our simulation(middle), and the simulation by the Soft-Robots plug-in for SOFA [5](right).

When new materials are used, the ratio R_m in Eq.(3.7) can be computed directly if their Young's modulus are known, or obtained through a tensile test as in Fig.3.5(b). Then, the shape parameter R_ω can be determined by Eq.(3.8).

3.5 Results

The proposed method of geometry-based direct simulation has been implemented in C++ and tested on a standard PC with an Intel i7 2.4GHz CPU and 8GB RAM. All the simulations can be run in an interactive speed (i.e., 4-5 fps) with a mesh size of up to 7.5k tetrahedra, which can be seen in the supporting video of this thesis. With the same configuration, the commercial FEM software Abaqus needs 1.5 minute to compute the deformation for a single frame, i.e, our result is 45 times faster.

The models of soft robot are digitally represented by tetrahedral meshes, and their corresponding physical objects are fabricated by the FDM 3D printer Ultimaker 3 which can print two materials in a build. The two materials used in our experiments are NinjaFlex and Flexible PLA with Young's modulus 12MPa and 45MPa respectively. Therefore, $R_\omega = 7.08$ is used for our simulation. Our results are compared with the SoftRobots plug-in for SOFA [5] and also verified with physical experiments.

3.5.1 Comparison with the SoftRobots plug-in for SOFA

To compare the performances between SOFA and the new framework, a cable-driven gripper with made of a single material is used as shown in Fig.3.6, which is fabricated with the Flexible PLA. The top and bottom rows show two sequences of deformations at different time instants. From left to right, the results of physical test, our simulation and SOFA are shown. Due to the fact that the deformation accuracy is traded off for computational speed in SOFA, its results do not match with the physical tests at large deformations. Specifically, the simulation starts to differ from reality when cable length change is larger than 45% or the chamber's volume change is greater than 30%. In contrast, our simulation can produce very realistic results while having a similar computational speed as SOFA.

3.5.2 Verification

To verify the result of the simulation for multiple materials, two cable-driven grippers with different material compositions were tested. The simulation and physical results are compared visually with its dynamics in the top and the middle rows of Fig.3.7. The deformations are also compared quantitatively by the trajectory of three corresponding markers located on the boundary of the grippers (i.e., P_1 , P_2 and P_3). It can be seen that both results match with the physical experiments very well. Another example has been shown in Fig.3.1 as a hand model compounded by a few manipulators with different material compositions. The results of simulation and physical test show a great match.

As presented in Section 3.3, this new framework can work not only for the cable-driven but also the pneumatic soft robots. One example is shown in Fig.3.8, and it is compared with the physical experiment by increasing the pressure of air pumped into the chamber to control bending of the gripper. From all these tests, it is easy to conclude the high accuracy of the new geometry-based direct simulation framework.

3.6 Conclusion

In this chapter, a new geometry-based simulation for soft robots was developed. The motivation of this work comes from the observation that the current actuations of soft

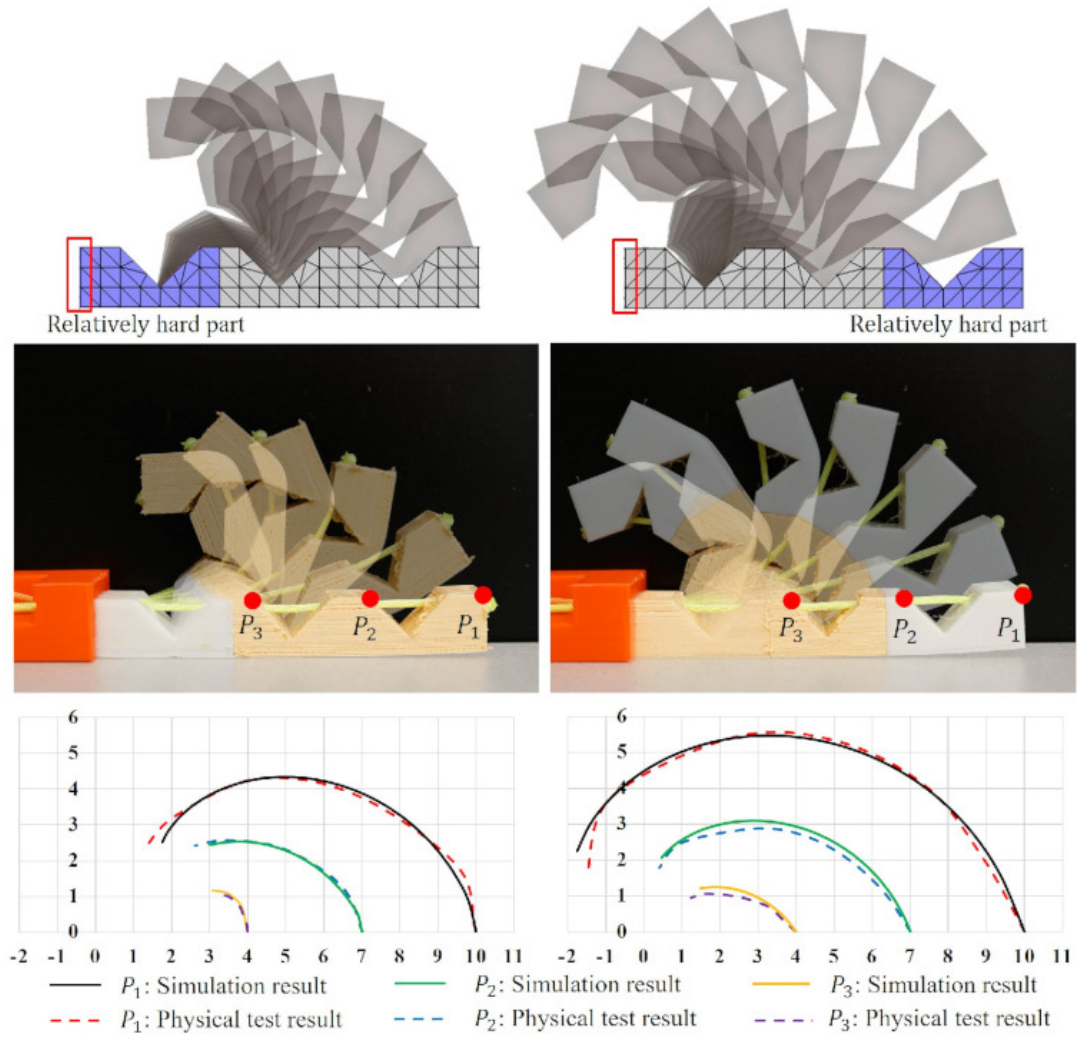


FIGURE 3.7: Two cable-driven soft grippers (left and right) with different material distributions have different behaviors under actuation. Locations of markers determined by our simulation are well-matched with theirs in physical test.

robots such as length shortening of cable and volume changing of chamber are based on geometry variation. In summary, a geometric optimization for preserving shape during deformation with the function of representing actuations as different type of geometric constraints to be imposed on specially designed elements was developed and implemented. Moreover, multi-material simulation is also supported by the framework with a well-designed calibration process for finding relative material properties. The experimental results support the hypothesis and verify that the proposed simulation framework is valid, direct, and promising.

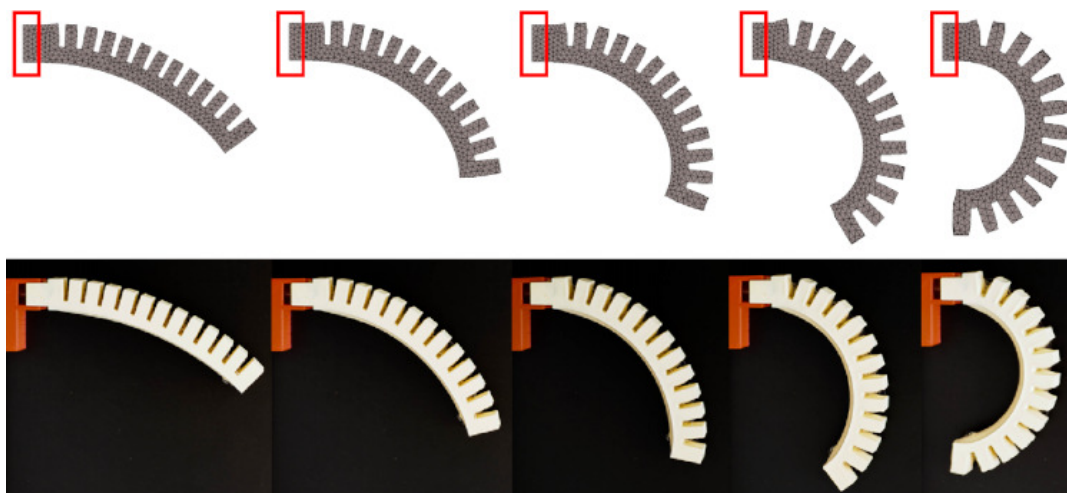


FIGURE 3.8: Pneumatic-driven soft gripper: (top) the results of our simulation and (bottom) physical test by increasing the pressure of air pumped into the chamber. The gripper is fabricated by the NinjaFlex material.

Chapter 4

Multi-Material

Digital-Light-Processing Printer

4.1 Introduction

To realize a practical multi-material DLP printer, a solution must be provided to the following research question: how to speed up the material swapping process and minimize the cleaning time without an increase in contamination?

In this study, it is observed that the material swapping in DLP printer is similar to a storage and retrieval process; and currently most of the cleaning systems are relatively passive (such as soaking). Trying to answer the research question based on these observations, two hypotheses are made:

1. If the material swapping is formulated as a storage system, it will speed up multi-material DLP printing.
2. If an active cleaning system is employed, it will enhance the cleaning effectiveness and efficiency.

Development of a multi-material DLP printer is created to test these hypotheses. However, there are several challenges in implementing the systems. On one hand, to maintain the robustness and simplicity of the printer, the integration of a storage system should not increase the process complexity too much. On the other, taking into consideration the safety and sustainability of the printer, the cleaning system should minimize the exposure of cleaning solution to the environment and conserve the material usage.

By overcoming these challenges, the contributions of this work are:

1. The techniques from automated storage and retrieval system (ASRS) are applied to develop a storage system for multi-material DLP printer. The whole system only has three axes of actuation and the time complexity of swapping is reduced from linear to constant.
2. The advantages of showering over bathing are taken and apply “running water” to develop a spraying mechanism that can effectively clean parts with complex features. The cleaning solution is recycled and kept airtight.
3. The whole system is sustainable and scalable. The design of the printer is modular and highly customizable, and the material waste for build materials and cleaning solution is minimized.

The theoretical analyses and experimental studies are also done to verify the functionality of the systems and test the hypotheses.

The rest of this chapter is organized as follows. Section 4.2 presents the material storage and retrieval system, and Section 4.3 outlines the cleaning system. Section 4.4 discusses the results acquired from the prototype. In the last section, the conclusion and the future work are presented. The hardware setup of the printer is given in Appendix B.

4.2 Material Storage and Retrieval System

One of the primary concerns with multi-material 3D printing, especially with DLP printers, is the time and the mechanism for swapping materials. This mechanism differs from other 3D printing processes since an entire container must be removed from the build area and replaced with another. Additional considerations are the storage density of the system, the scalability in terms of build area and number of materials, as well as the complexity of the printer. Although swapping and storage mechanisms have been used in many industrial applications, they have particular requirements and use cases which do not easily translate over to the DLP process. While some existing methods [17, 18, 45] use linear or rotary stages to swap different materials, they have poor scalability and suffer from long material swapping time. To

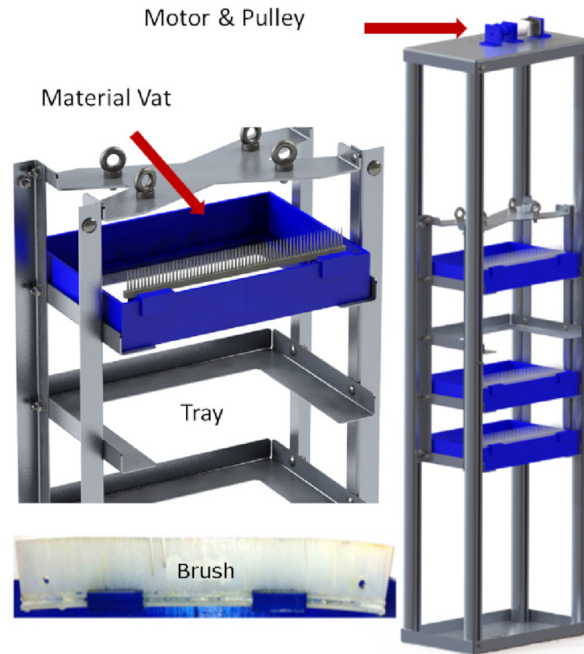


FIGURE 4.1: Material tower with vats and silicone brush

address this problem, the objective here is to apply the techniques from automated storage and retrieval system (ASRS) to establish a material storage and swapping system for multi-material DLP printing. The storage system is discussed first, and it is followed by the swapping mechanism.

4.2.1 Storage System

The common geometry for a material vat is having rectangular shape or is a circular disk for experimental setup. To maximize the print size, the rectangular vat is employed in this study as depicted in Fig. 4.1. Observing that the material vat is a boxlike storage compartment without a lid, a drawer design that is made to slide horizontally in and out is employed for the storing process, and a material tower as shown in Fig. 4.1 is developed to provide a high-density vertical storage solution. A vertical approach is desired because of the fact that material vats have much greater length or width than they do height, as such not only can storage be more dense and efficient, there is also less distance that needs to be traveled to access the next material. A stepper motor and pulley at the top of the tower is used to raise and lower the trays holding the material vats. The detailed hardware setup of vertical storage tower is described in Appendix B.3.

Although the design is simple, it is sufficient to test the first hypothesis of employing ASRS in multi-material DLP printer. Due to the vertical and independent nature of our current design, to be able to access the top most material, there needs to be enough room on the bottom of the tower to accommodate the other materials. In the current design, 4 inches of clearance was given between each material. Following these measurements, 8 additional inches would be required for one more material. The current height of the prototype tower is 60 inches and can accommodate 8 vats. Compared to the rotary design [18] which housed 2 materials, this design hosts more materials. More importantly, the rotary design needs to fit a number of material vats in the circular platform, the size of which varies greatly with the size of vats and the number of materials. This may limit proper industrial implementation. In contrast, our design has much better extensibility and has an effective use of floor space. In terms of packing density, which is calculated by dividing the volume of the vats by the volume of the storage solution, our design can achieve a factor of around 0.6 while the rotary design is only about 0.3, for the same number of materials with similar print size.

The packing density can be improved in the future by incorporating a vertical carousel storage system to rotate with multiple towers, so that no empty space is needed within the tower.

The tower with adjustable partitions and dividers is modular and highly configurable. The number of trays, thus available materials, can be modified with minimal additional design work by simply changing the length of the corner extrusions. Moreover, increasing the build area of the printer changes the size of the vats. For the vertical tower design, only the top and bottom braces as well as trays need to be resized to accommodate such changes, see Fig.4.1. The use of common stock materials, a simplistic design, and designing for manufacturing makes the storage solution easily scaled to the required size, and for the desired number of materials.

4.2.2 Material Swapping

In a linear design, both horizontal and vertical configurations, the complexity of material swapping is directly proportional to the number of materials, i.e., $O(n)$ where n is the number of stations on the conveyor. In other words, the worse case scenario

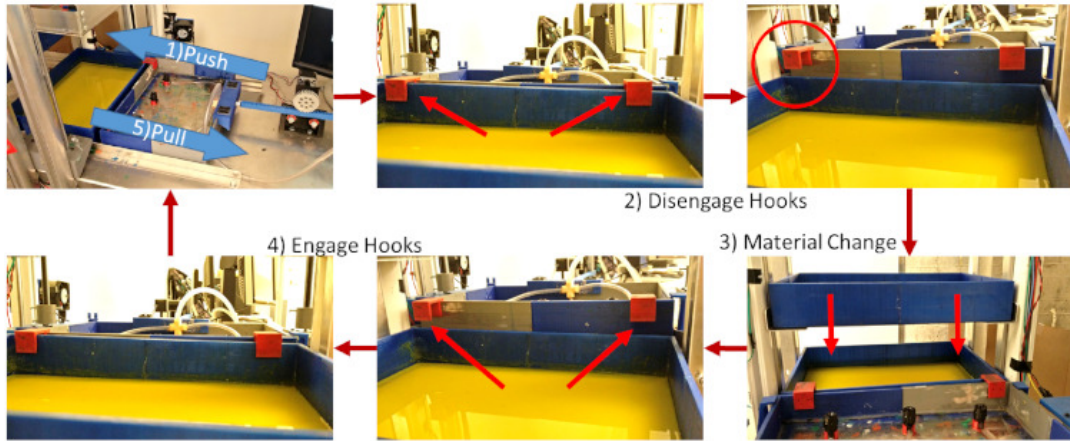


FIGURE 4.2: Material swapping process: 1) The material swapping process starts with the cleaning vat pushing the material vat into the tower. 2) The tower lowers to disengage the hooks. 3) The cleaning vat moves back to allow clearance of the hooks, and the tower selects the next material. 4) The material vat advances and the tower rises to engage the hooks. 5) The cleaning vat pulls the material vat into place

is changing material from one end to the other. This requires it to pass through every station on the conveyor in order to get to the next material. A rotary design is better as it can turn the table in either clockwise or counter-clockwise direction, but the complexity is still linear. Due to the necessity of moving entire vats in and out of the print area, it is impossible to completely eliminate swapping time. However, because the swapping and cleaning do not need to be related to each other, they can be decoupled in the design of the storage solution, and it is possible to set the next material vat in the ready position while the cleaning process is underway. Compared to the previous work of [45], this decoupling is the largest increase in efficiency.

As the material tower is a vertical lift system, we design a storage/retrieval (SR) machine that can push and pull the material vats from the tower. Actually, the SR machine is permanently attached to the cleaning vat (explained in Section 4.3), such that the positioning of the cleaning vat is combined with the material swapping. It is worth noting that it is a compact and efficient design which can accomplish material storage/retrieval and cleaning by one single degree of freedom (X -axis) without the need of complex controls. The procedure created to swap materials has several steps and is illustrated in Fig. 4.2. First, our storage solution, the vertical tower, should already be in the receiving position with an empty tray aligned to the printer platform. A rack-and-pinion mechanism then pushes the vat onto the tray and into the tower.

Guide rails on either side ensure proper alignment. In this sense, as the material vat goes into the tower, the cleaning vat is also moving into its cleaning position. The cleaning vat is equipped with the red hooks which are used to latch onto the material vats. Once the material vat is properly inserted, the tower lowers to disengage the hooks and the cleaning vat is pulled away to prevent interference. With the material vat in the storage system, it is free to rearrange the materials, which allows the tower to position the next material while the part is being cleaned. After cleaning is complete, the cleaning vat moves forward to receive the next material vat. The tower then raises to engage the hooks and the new material is pulled into place. The following layer is now ready for printing. In this way, the complexity of the process is constant, i.e., $O(1)$. This supports the first hypothesis and the tower-based ASRS speeds up the material swapping process for multi-material DLP printing from linear complexity to constant.

4.3 Active Cleaning System

Another challenge in multi-material DLP printing is the cleaning of residual resin on the build part and bed. If the previous uncured material is not removed, contamination happens on both the part and the vats containing other materials. There are a number of considerations in the cleaning system: cleanliness, material usage and waste, speed, size and scalability of the cleaning system, as well as the evaporation of the cleaning solution. The proposed method must also be able to reach complex geometries.

The existing systems for cleaning are using a cloth to wipe the printed part [49] and soaking the part [18]. The cloth method is fast but it is unable to deal with intricate geometries. In addition, the process would have to be done manually which is undesirable and inconsistent. It is more promising to soak prints in isopropyl alcohol for several minutes, anywhere from 5 to 20 minutes depending on the resin used [50]. The purpose is to dilute and clean the excess resin from the print before further operation. In this sense, utilizing an ultrasound machine in conjunction with the cleaning agent would further increase the efficiency of the process. The ultrasound method adds vibrations to the cleaning solution which in turn leads to cavitation.

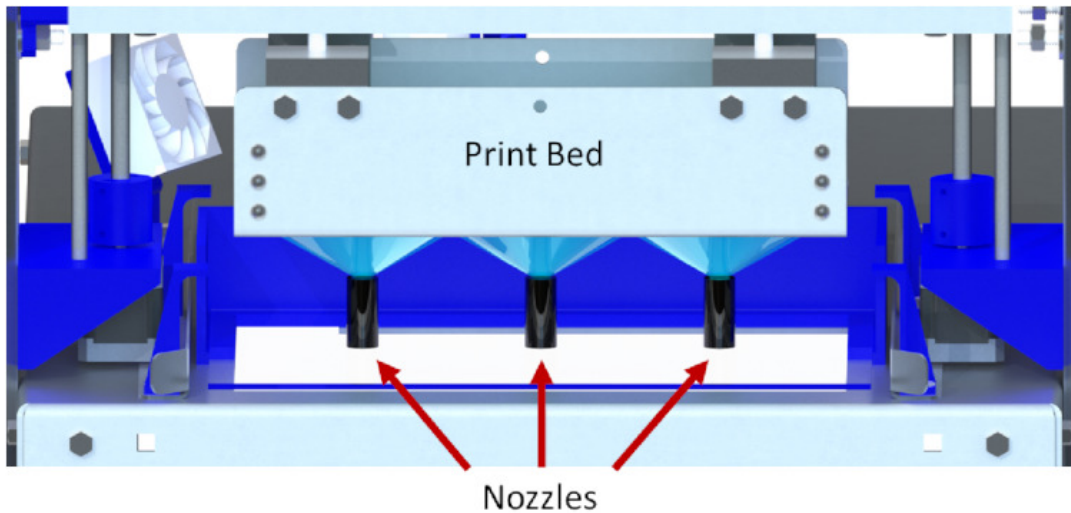


FIGURE 4.3: Spray pattern of the 3 sprinkler heads

This effect causes bubbles of air to implode on the surface of the part and dislodge the contaminant [51].

In terms of cleanliness, the soaking method would become less and less effective with every cleaning step, since the cleaning agent would become more contaminated. Furthermore, having a large bath constantly exposed in ambient air would lead to excess evaporation, bringing additional concerns to size and scalability of the approach. Therefore, our goal is to develop an active cleaning system to have the contaminants running off from the part and down into a filtered drain with the cleaning solution, such that the aforementioned considerations can be achieved.

4.3.1 Spraying Mechanism

Showering is known to have advantages over bathing such as being more environmental friendly, less cleaning time, and cleaner. Learning from showering, here we develop an active cleaning system that utilizes three sprinkler nozzles and a pump to spray the part. Once the material vat has been placed in the tower and the cleaning vat positions itself under the print bed. The pump then turns on and the cleaning solution is ejected from the sprinklers. This is a direct approach to deliver the cleaning solution onto the print bed and hit the part in places that are hard to reach.

The spray pattern is angled towards the part as can be seen in Fig. 4.3. To ensure proper coverage of the print bed and piece, the cleaning vat oscillates from side to side in the X direction while the print bed rises and lowers. The spray itself

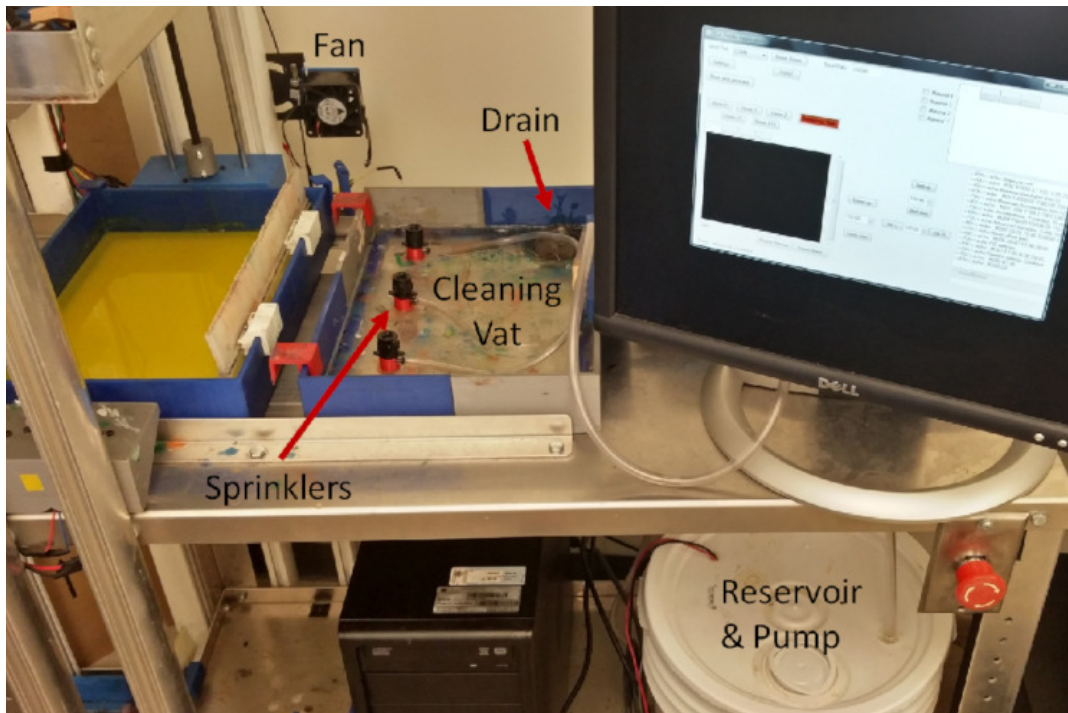


FIGURE 4.4: Cleaning system: sprinklers, brush, drain and reservoir

is similar to a heavy mist in a cone. Additionally, this system is easily scalable for larger build volumes by adding/removing sprinklers or simply adjusting the positions of the sprinklers. The spray method combines both the cleaning power of the cleaning solution with the impact force of the spray. Consequently, this also creates movement of the cleaning solution which means it is further able to penetrate complex geometries and cycle the solution so that resin can escape from crevices. This theoretically decreases the exposure time to the cleaning system, and increases the efficiency of the cleaning solution. This is important because prolonged exposure to the cleaning agent can cause swelling in the printed part and affect print quality and accuracy [52].

Proper tuning of the pump is done to ensure there is enough pressure to spray the parts but not too much such as to damage the part. After cleaning is complete, the cleaning vat then moves into position to pull the new material into place while fans angled towards the print bed help dry the print for the next layer.

4.3.2 Sustainability

Both the resin and the cleaning solution are consumables that the cleaning process uses up. Minimizing the waste of these materials is crucial to reduce the cost and

improve the sustainability of the system. In addition to the spraying mechanism that reduces the amount of cleaning solution being used, two other components are also incorporated in the system: a silicone brush and an airtight reservoir. The silicone brush is integrated into the material vat, as seen in Fig. 4.1, and the reservoir houses the cleaning solution with a diaphragm pump which supplies the sprinklers. The reservoir is also connected to the material vat where the resin and the excess cleaning solution can be drained after spraying. The general layout of the cleaning hardware and system can be seen in Fig. 4.4.

Because all the uncured resin dissolved in the cleaning solution will be material waste, a substantial cleaning is done by the silicone brush installed in the vat. Silicone was used so that none of the resin gets absorbed by the brush, and placed within our material vats so that all excess resin that is wiped off is directly returned to its vat, which further reduces waste and initial resin required at the start of the print. Additionally there is no risk of losing bristles during the cleaning. Whenever material swapping is required, the print bed raises to a height such that the silicone brush can make contact with the contaminated area to remove and recuperate as much resin as possible back into the material vat. This cleaning is performed implicitly when the rack-and-pinion pushes the material vat back into the tower, and thus no additional time is required.

The cleaning solution used, and recommended for cleaning resin, is an isopropyl alcohol-water mixture of 90%-10% [17]. This means that leaving a large vat exposed would lead to quick evaporation of the solution, filling the environment with dangerous fumes. As such, the proposed system uses an airtight reservoir (Fig. 4.4) with a pump submerged to supply limited amounts of cleaning solution when needed. The excess resin and solution is recollected and recycled through a drain, made of a filter and funnel, placed in a corner of the cleaning vat which feeds back into the reservoir, so that the amount of alcohol evaporated can be minimized.

4.4 Results

There are two hypotheses, one regarding material swapping and the other regarding active cleaning. To test the hypotheses, a prototype multi-material DLP printer was

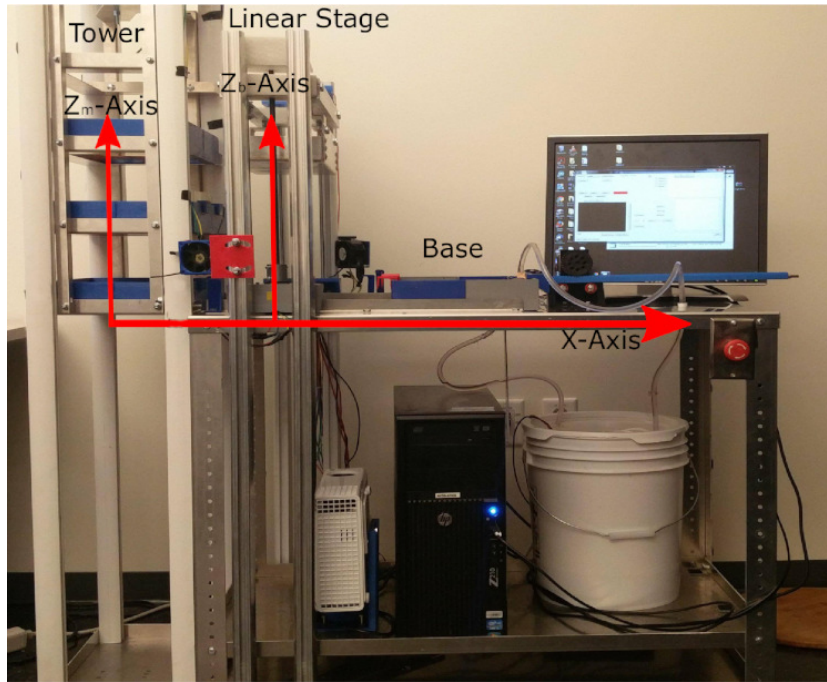


FIGURE 4.5: Multi-Material DLP Printer Prototype

built as shown in Fig.4.5. The overall hardware and software architecture is available in Appendix B. The printer uses a bottom up approach to limit the contact of the printed part and the resin. The printer consists of three degrees of freedom: build platform (Z_b -axis), material tower (Z_m -axis), and rack-and-pinion (X -axis). A custom C# application was developed to handle the sorting algorithm and control the prototype based on the RepRap framework [53]. A piece is first designed as separate bodies and sliced individually to generate a set of black and white images for each material. Once a layer is printed for one material, it checks if there are images for the other materials. If there is, it initiates the swapping process, else it prints the next layer.

A series of different parts with varying features were printed to test this system, and duration of both the exposure time to the cleaning system as well as the drying times were determined experimentally, the results of which are presented in this section. All tests were preformed with the G+, and semi-flex resin from MakerJuice [54]. Some of the fabricated multi-material examples are shown in Fig. 4.6 to validate the correctness and functionality of the system. Furthermore, we compare our method with the previous work [18], and Table 4.1 summarizes the key differences including the number of materials for the two prototypes, the build area, the time it takes to



FIGURE 4.6: Examples of multi-material prints: A) 4 colored die; B) Ball in a cage with two colors; C) Concordia printed in 3 colors on a semi-flexible backing.

TABLE 4.1: Comparison of previous prototype and ours

Prototype	Zhou et al. [18]	Our
Build Area	6 in^2	72 in^2
# of Materials	2	8
Swapping Time	180s	62s
Cleaning Time	120s	15s

swap from one material to the next, and the cleaning time. The cleaning percentage is the average of the testing presented in Section 4.4.2. In the following, the quantitative comparison will be presented in detail.

4.4.1 Material Swapping

In Section 4.2, we have discussed the theoretical speedup that could be achieved with the tower-based design, and this section is going to present the experimental data. With the current configuration, the material swapping cycle includes part of the cleaning cycle. In this sense, both subsystems are paired together to save time overall and increase the efficiency of the material swap. Additionally, by allowing the storage system to select the material independently, the rest of the printer is free to perform any other task, in this case, spraying and cleaning the print bed. Finally, by making every operation linear, the scalability of the solution is ensured. As the print area increases or decrease, the travel distance follows in a one to one ratio, and as the number of materials increase, it does not affect the material swapping time. Fig. 4.7 illustrates each of these individual processes and when they occur relative to each other

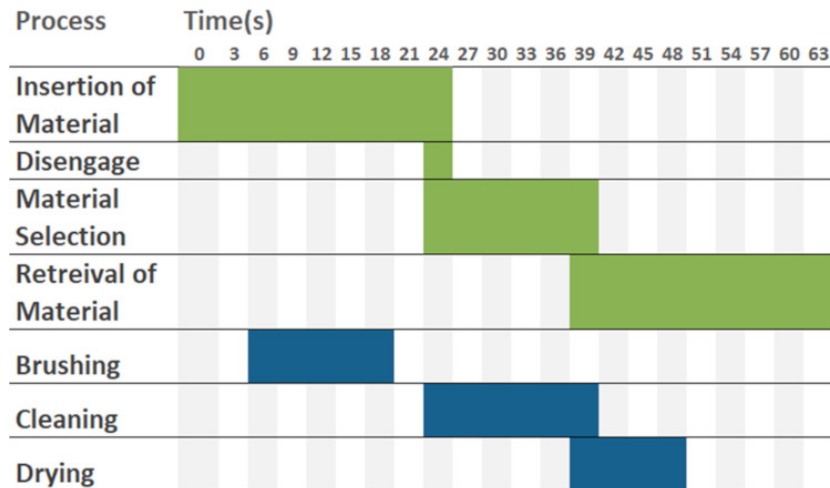


FIGURE 4.7: Figure shows the breakdown of the varying steps within the material swapping process. In green are the tasks that involve moving and swapping the material vat. In blue are the steps involved in the cleaning process

throughout a complete material swap and cleaning. The time for the brushing phase of the cleaning process is partially dependent on the speed of the material storing process, however it is still displayed as its own process because it helps to demonstrate clearly the total time required to clean the part effectively. From the figure, the total material swap time takes 63 seconds. The insertion of the material as well as the retrieval process take up the majority of the time at 24 seconds each. Both processes are affected by motor speeds of the X -axis as well as the distance needed to travel due to the size of the print area. The material selection time of the prototype takes 15 seconds. The disengage time, 3 seconds, is illustrated as well since it is still possible to optimize the hook geometry or use a system, such as electromagnets, to reduce the time. The previous work [18] had an approximate swapping time of 180 seconds, and there is a $3\times$ improvement in speed for our prototype. Although it may not sound significant, it should be noted that there is a huge difference in the build area, i.e., $6in^2$ [18] vs. $72in^2$ in our case. Therefore, the proposed solution is three times faster while having a build area that is twelve times larger. These results support our first hypothesis that applying ASRS can increase the material swapping speed for multi-material DLP printing.

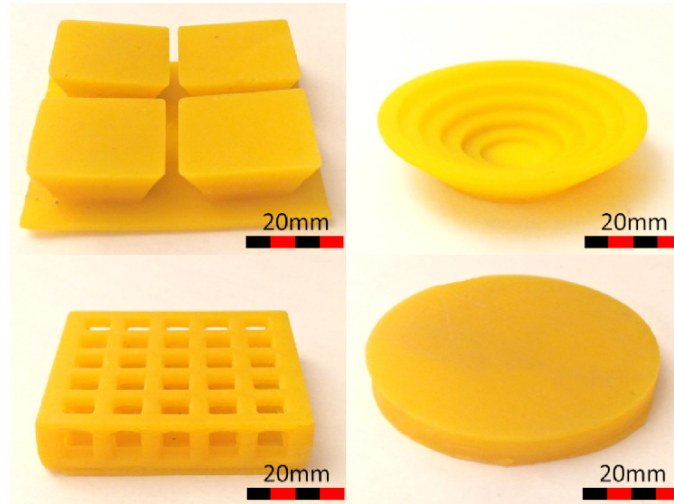


FIGURE 4.8: Pieces used for contamination test. Top left: Four inverted Pyramids . Top Right: Staggered Cone. Bottom Left: Scaffold. Bottom Right: Cylinder

4.4.2 Cleaning System

For a successful cleaning system, contamination must be as close to zero as possible. This condition takes priority over total print time as multiple material changes will continuously accumulate to the total amount of contamination during a print. To determine the effectiveness of the proposed active cleaning system, a residue test is conducted to compare the amount of residue left on the part by different methods.

The residue test involves printing pieces with varying geometries and features, and weighing them after the print. The geometries of the parts were designed to represent different features to clean and test the cleaning system capability to deal with overhangs, hard-to-reach surfaces, cavities and complex geometries. Pictures of the testing samples cleaned by the spray system are shown in Fig. 4.8. Increasing the vertical surfaces and overhangs ensures cleaning systems have to be able to reach the entirety of the piece. Smaller features and intricate cross sections, such as the scaffold, create large amounts of cavities, and surfaces that continually get contaminated and covered by subsequent layers and thus more difficult to clean.

These pieces were printed and weighed when exposed to 6 different scenarios. Firstly, it is weighed without any cleaning thus being the most contaminated piece. Secondly, it will then sit in a bath of alcohol for two hours to ensure that all resin has been diffused from the part and will act as the basis for a completely cleaned part.

TABLE 4.2: Contamination test results, weight in g. U/S = Ultrasound

Piece	No Clean	Full Clean	Cloth	U/S (15s)	U/S (120s)	Spray (15s)
Cone	8.10	7.21	7.99 (12%)	7.86 (27%)	7.74 (40%)	7.22 (99%)
Scaffold	16.40	15.20	16.31 (7%)	16.30 (8%)	15.60 (67%)	15.30 (92%)
Cylinder	15.60	14.90	15.12 (69%)	15.39 (30%)	15.32 (40%)	14.92 (97%)
Pyramids	17.00	16.21	16.79 (37%)	16.55 (27%)	16.3 (57%)	16.28 (91%)

In the third scenario, the contaminated pieces are be wiped using a cloth [49] to see its effectiveness. The fourth and fifth cases expose the pieces to the ultrasound (U/S) bath for 15 seconds and 120 seconds [18], respectively. Sixth, the pieces are exposed to the proposed spray cleaning system for a single oscillation of the cleaning vat lasting 15 seconds, this ensures the cleaning solution covers the entirety of the print bed. The fourth scenario is designed to be compared with the sixth one to illustrate the effectiveness between passive and active cleaning for the same amount of time. The difference in weight between each trial and the fully cleaned part will be the excess resin, and thus the level of cleanliness. Results of the residue test can be seen in Table 4.2 where the percentage illustrates the cleanliness of the piece.

Table 4.2 shows that using cloth to wipe a printed piece will give varying results based on the geometry. Although the method is very fast, at 5 seconds to perform, its performance is inadequate. The ultrasound bath performed better than the cloth in every scenario except the cylinder which predominantly has a one flat face which favors wiping. It can also be observed that exposing the contaminated part for longer in the ultrasound bath, first 15 seconds and then 120 seconds, did reduce contamination but with varying results. By comparison the proposed active cleaning system utilizing the spray of a cleaning solution reduced contamination to as low as 0.1g from the full clean piece in 15 seconds, which results in parts that are over 90% clean. The proposed method outperforms the passive systems in cleanliness and time required.

The previous cleaning systems, using ultrasound [18] and cloth [49], reported that they took 3 minutes and 2 minutes for cleaning respectively. Comparatively, the prototype system takes only a total 25 seconds for the whole cleaning cycle to achieve

a nearly full-clean result, which is an order of magnitude faster than both systems. This experiment supports the second hypothesis that an active approach to cleaning resin results in low levels of contamination and a significant reduction in cleaning time.

4.5 Conclusion

A new method for multi-material DLP printing has been presented. To increase the efficiency of material swapping, the technique from automated storage and retrieval system was used to design the material swapping mechanism which utilizes a tower as a storage system and the retrieval system is coupled with the cleaning system, so that the overall process complexity is just three degrees of freedom. An active cleaning approach was then devised using sprinklers to deliver the cleaning agent to clean the build part in-between the material swapping. The prototype was then tested to prove the merits of these solutions. By decoupling of the material swapping and cleaning systems, it allows for independent optimization as well as an increase in efficiency of the overall system. The prototype showed a swapping time of one minute between vats, and a cleaning time of 15 seconds. Due to the prototype being a proof of concept, several components, while functional, are not fully optimized. There are a number of things that could be improved.

Chapter 5

Conclusion

This thesis has presented a new formulation to simulate soft robots as well as a novel method for the 3D printing multi-material soft robots utilizing the DLP method. By understanding that soft robots are actuated by a change in geometry it is possible to develop a framework which is efficient and accurate. New element types are defined to represent the actuations, be it the shortening of a cable, represented by a triangular element, or the enlarging of the bowels represented by a volumetric element. These elements then act as constraints which enable the iterative deformation of the soft robot. This has been proven to reproduce accurate results when compared to both Abaqus and experimental tests, while achieving a 45x speeds increase. When compared to other soft robot solvers, the new framework provides more accurate results at large deformation, and allows for the use of multiple materials. The framework has been demonstrated by cable-driven and pneumatic-driven soft robots, but it will be extended to other actuations and be able to model multiple-actuations simultaneously. Another future work is to extend this simulation for soft robots that are made up of more than two types of materials. One way to do this, is to introduce more degree of freedom in the calibration of shape parameters. In addition, non-linear material models, such as hyperelastic materials, are also being investigated. This would mean the framework is addressing non-linearities in a completely local manner, which would allow the framework to continue being efficient by not needing to update the global stiffness matrix. Finally, due to the high computational speed and efficiency of the solver, it would be possible to develop inverse kinematic models for the soft robot by iterating through forward kinematic configurations. This would provide a complete solution to soft robotic simulation and address the current bottlenecks in the field.

To be able to fabricate these soft robots with increasing levels of geometric complexity, new manufacturing methods needed to be investigated. Traditional methods such as molding are limited in geometry and present a complicated process when dealing with multiple materials. 3D printing has been gaining traction with their ability to recreate such geometries even with elastomeric materials. The current solutions on the other hand, posed several unique problems or limitations. FDM machines were highly anisotropic and had low tolerance on printed parts compared to other methods. While poly-jetting had poor fatigue properties due to the manufacturing process. As such DLP printing was deemed a promising method to create multi-material soft robots as the manufacturing speed was high, while the coalescence is the best among the other options. DLP brought its own set of challenges such as contamination between materials, the swapping process since complete vats need to be displaced, as well as the number of materials per print and the overhead time for dealing with multiple materials. The problems with contamination was addressed by utilizing a more active cleaning approach using jets of cleaning agent. While the swapping of materials and the inherent time loss, was addressed by adapting classical automated storage and retrieval systems to a DLP printer. This led to a 3x speed increase for the total system, while dealing with a print area that is 12x larger than the previous solutions.

The current speed of the material-swapping process is dependent on the size of the print area, as well as the speed of the stepper motors selected. Upgrading motors could drastically affect travel times as well. The latching mechanism could also be improved to eliminate any additional displacement by using electromagnets. The current spray pattern functions but is rather simple, optimizing the spray pattern could result in faster cleaning time and less solution being used. In addition, the effects of cleaning solution and swapping mechanism on different part geometries, accuracy and material properties are to be investigated. To start challenging the likes of FDM and Polyjet printers in terms of available maximum materials per print, an improved storage system would have to be developed to allow more towers to be interchanged during the course of the print or have a wall of vats with an independent system to retrieve the desired material. Additionally multi-material DLP printing requires a more complete software solution. This would mean a new slicing program to efficiently generate the

image files and generate the required g-code to control the printer.

These two branches of research are working in parallel to allow the development and further research into soft robots. By making the simulations faster and more accurate, it would allow designers and researchers to virtually actuate their robots before going through the complex steps of manufacturing. This also allows them to optimize their design while still in the conceptual phase. This drastically departs from the approach of trial by error which is being used for soft robots. With inventive designs becoming more prevalent, the manufacturing methods must also be improved. The ability to have homogeneous properties that are unaffected by the manufacturing method means the desired robot is what is obtained. Further development of the DLP method, as well as new materials being created will allow for limitless designs and accurate reproduction of the digital model. Due to this, innovation can continue in terms of exploration robots which can deal with more situations, more realistic and complex prosthetics, as well as mechanically programmed compliance for dexterous tasks.

Appendix A

Local Global Solver

The algorithm used to compute the final mesh \mathcal{M}_s^f is described in a local-global iterative way. Firstly in the local step, a pure rotation transformation matrix \mathbf{R} is computed from the current shape \mathbf{V}_i^c to target shape \mathbf{V}_i^t for every geometric element. After that, by centralizing into local coordinates the final shape \mathbf{V}_i^f for this iteration is computed by combining the rotation matrix \mathbf{R} with the current shape \mathbf{V}_i^c . Finally those dispersed geometry elements are assembled into a global system by solving a least-square optimization problem to get the final mesh \mathcal{M}_s^f . The computation is dynamic, local and global steps are run in a iterative way until the system energy converges.

A.1 Local projection step

The goal of this step is to find the pure rotation matrix \mathbf{R}_i for every geometric element \mathbf{V}_i from current shape \mathbf{V}_i^c (acquired from last iteration result) to target shape \mathbf{V}_i^t . For constrain element, target shape is defined to satisfy the corresponding constraint. As for unconstrained elements, target shape is calculated first based on the material properties present, this will be discussed in section 4. Here the target shape is assumed to be known and pre-processed.

From \mathbf{V}_i^c to \mathbf{V}_i^t a linear affine transformation matrix \mathbf{T} is defined along with a displacement vector \mathbf{d} as

$$\mathbf{T}\mathbf{V}_i^c + \mathbf{d} = \mathbf{V}_i^t \quad (\text{A.1})$$

By introducing $\mathbf{P}_c = [v_1^c - v_2^c, v_1^c - v_3^c, v_1^c - v_4^c]$ and $\mathbf{P}_t = [v_1^t - v_2^t, v_1^t - v_3^t, v_1^t - v_4^t]$ the effect of \mathbf{d} can be displaced and calculate \mathbf{T} by minimizing:

$$\sum \|\mathbf{P}_t \mathbf{P}_c^{-1} - \mathbf{T}\|_F^2 \quad (\text{A.2})$$

After that by using singular value decomposition (SVD) method this transformation matrix becomes $\mathbf{T} = \mathbf{U}\mathbf{\Sigma}\mathbf{V}^T$. The pure rotation matrix can be presented as $\mathbf{R} = \mathbf{U}\mathbf{V}^T$.

A.2 Global assembly step

In the local step the transformation matrix is obtained for different situations, and they are used to calculate the final shape of every element. Here in global step they are being assembled into a larger system based on the continuity of mesh \mathcal{M}_s while minimizing the difference between current shape and target shape for the whole system. Here the optimization energy function for a single element can be described as:

$$E_i = \|\mathbf{N}\mathbf{V}_c - \mathbf{N}\mathbf{V}_i^t\|_F^2 \quad (\text{A.3})$$

where \mathbf{N} is a 4×4 matrix used to shift the tetrahedral into origin coordinates in order to eliminate displacement differences between elements. Here $\mathbf{N} = (n_{i,j})$ is defined as

$$n_{i,j} = \begin{cases} 3/4 & \text{if } i = j \\ -1/4 & \text{if } i \neq j \end{cases} \quad \forall i, j \in (1, 2, 3, 4).$$

Consider all the boundary condition as projection, Equation 3 can be reformulated with the presence of vertex position as

$$E = \sum_{i=1}^m \omega_i \|\mathbf{N}\mathbf{V}_c - \mathbf{N}\mathbf{V}_i^t\|_F^2 = \|\mathbf{A}\mathbf{V} - \mathbf{p}\|_F^2 \quad (\text{A.4})$$

where \mathbf{A} is a sparse matrix containing all the mean-centered items, \mathbf{V} is the final shape for the mesh and \mathbf{p} is the summary of all projected target shape elements. The weight ω_i for the unconstrained area is equal to one. However, for constrained elements it is used to describe how hard the constrain is (discussed in Section 3). By

setting the derivative of Equation 4 as zero the minimization problem can be solved as $\mathbf{A}^T \mathbf{A} \mathbf{V} = \mathbf{A}^T \mathbf{p}$. Notice that matrix \mathbf{A} only depends on N to describe the stiffness of the system so that $\mathbf{A}^T \mathbf{A}$ can be pre-factorized and reused in all iterations as long as the connectivity of mesh has not changed. Based on these steps, the new final mesh \mathbf{M}_f generated by \mathbf{V} can be solve by backward substitution.

The two steps run in an iterative way and will make the energy E constantly decrease until the system converges.

Appendix B

Printer Architecture

The printer is broken down into five main components: printer base, build platform, material tower, cleaning hardware and the electronics/software.

B.1 Printer Base

The base of the printer, shown in Fig. B.1, is the main foundation to connect all the modules. The printing and cleaning process take place on the top level, while the second and third house the equipment. All other subsystems are attached directly to the base. The systems integrated into the base are as follows:

B.1.1 Top level

The top level accommodates the vat displacement and movement control. In order to move the vats on the top level (for shearing and material swap operations), the X-axis is driven by a geared stepper motor using a rack and pinion system. The rack-and-pinion uses a herringbone design to self-align and is attached to the cleaning vat using a printed hook. In addition, two rails are attached on the surface to help guide the vats. An opening is cut through the top level to allow the projected image to cure the resin through the material vats glass bottom. A second cut is performed to accommodate the cleaning vat drain, as well as a hole above the reservoir to pass the primary cleaning hose.

B.1.2 Middle level

The middle platform houses the projector, whose position and height is adjustable, and an airtight bucket which acts as a reservoir. The adjust-ability is threefold: The first

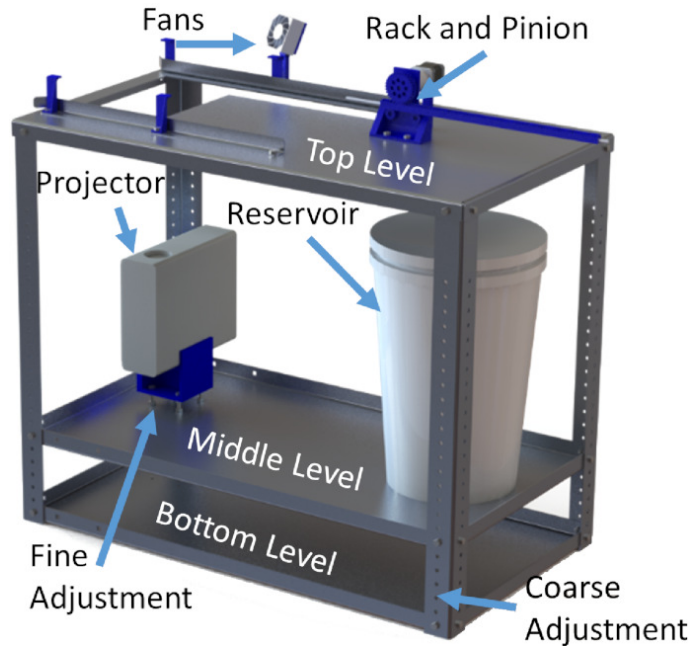


FIGURE B.1: Printer base with detailed components and sectioning

adjustment is the vertical position of the middle tray using the hole pattern on the four base legs (Fig. B.1). This is a coarse adjustment wherein the projector can be moved closer or farther away by one-inch increments. The second adjustment is for higher precision and accomplished by a alignment stage setup on the projector support. The support has four mounting points so that the proper angles and focal distances can be attained. Finally, it is noted that as the projector is moved up or down, the projected image also shifts location. As a counter measure, slots are provided in the tray to accommodate horizontal displacement of the projector to ensure a centered image on the print bed.

B.1.3 Bottom level

The bottom of the base is used to store and organize some of the electronics that will be outlined in section B.5. This includes the arduino, ramps board, as well as the power supply. Build materials can also be stored in this level.

B.2 Build Platform

The print bed shown in Fig. B.2 is a 12 by 6 in^2 surface made from aluminum sheet metal. The bed is attached to two L-stock extrusion cross beams. The bed level can be

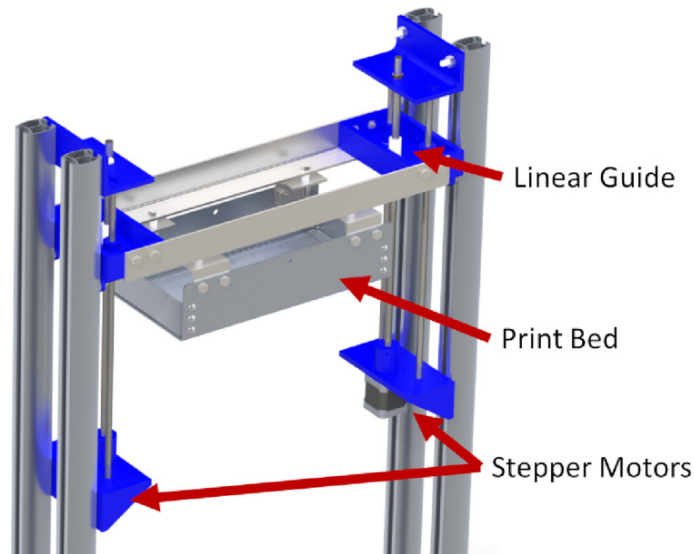


FIGURE B.2: Parallel linear stage with build platform

adjusted by varying the height of the four bolts fastened to the L-stock corners. The cross beams are anchored to two linear guides, each of which has a 10mm lead screw and two guide rods with linear bearings. The build platform displacement is controlled by two synchronized stepper motors, each turning a lead screw. The prototype print height is 12 inches.

B.3 Material Tower

The material tower system is designed to be a simple solution that allows the printer to easily store and retrieve the desired materials for any given print layer. The tower itself is built using four t-slot aluminum extrusions for the corners. The extrusions are held together with top and bottom flanged sheet metal plates with holes for fastening. Within the frame are trays that support the material vats. The sides of the trays are bent up to secure the vats in place. They have holes in each corner for attaching to a rail which is in turn guided by the t-slot extrusions during movement. To move the trays up and down, a geared stepper motor is mounted to the top bracket. The motor spins a small spool with a nylon strap attached to the trays.

B.4 Material Vats

The vats are rectangular with borosilicate glass laid down onto a plastic frame. A layer of polydimethylsiloxane (PDMS) is used as a non-stick coating to protect the glass and printed parts. The mask images will be projected through the glass to the print bed. The prototype tower supports four vats, each of which have an internal volume of 234 in^3 . The overflow of the resin has to be considered once the bed is submerged, therefore the maximum resin will be the volume of the vat minus the bed volume which is calculated to be 44 in^3 . Depending on the material quantity needed, the vats can have the same resin in two or 3 vats to increase print size. A silicone brush is attached to the inside of the material vat for cleaning purposes.

B.5 Electronics and Software

The electronics and control system design is based off of a DIY RepRap project, and it is an easy to replicate system that could be adapted for different printers [53]. The electronics system is composed of the following: A computer, an Arduino Mega 2560 R3 microcontroller, a RAMPS 1.4 board, a 12 V power supply, three limit switches, four stepper motors, two fans, a diaphragm pump and an emergency stop. Stepper motors equipped with a 99:1 planetary gear box are used to run the rack-and-pinion (X -axis) and the material tower (Z_m -axis), while two low-current stepper motors are used to control and run the vertical motion of the build platform (Z_b -axis).

The firmware that controls the printer operations on a system level is a fork of the popular open-sourced 3D printer firmware Marlin. This code base was selected primarily due to its compatibility with the RAMPS hardware interface. Adjustments to the firmware were made in order to accommodate the multi-material functionality of the printer. The peripheral devices of the printer, such as the pump and fans for the cleaning system, were wired to some auxiliary ports, so that no additional electronic or control component is needed. Marlin uses the popular CNC communication protocol known as G-code. A custom Windows Forms application was written in C# in order to control the movement of the printer and synchronize the projection of the layer images. The user interface is presented in Fig. B.3 with the key elements being denoted. G-code commands are sent via USB serial communication in real time while

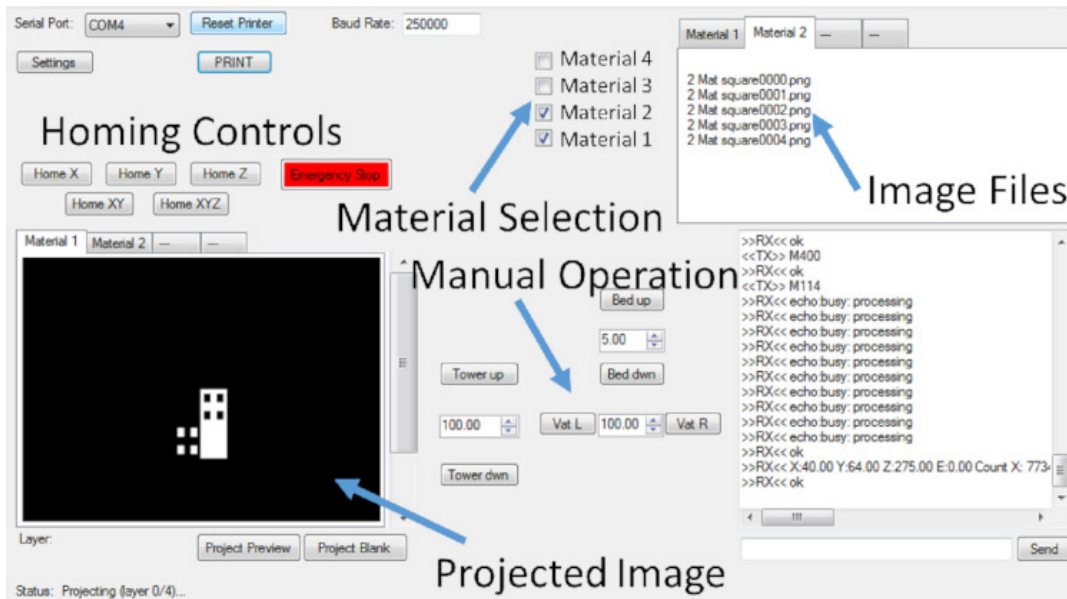


FIGURE B.3: Custom software depicted during operation

the Windows application processes the next move sequence. Models are first ported to a program called Creation Workshop which slices the models into png images. These images are then loaded into the software where the logic of controlling the printer happens. If a folder of images contains any blank or black images then the material is not present on the current layer, and the software skips it. If the last material printed on the current layer is also present on the next layer then it will be processed again before switching materials.

Bibliography

- [1] Sam Davies. Sailner exhibits multi-colour and multi-material 3d printing capabilities at tct asia, 2018. <https://www.tctmagazine.com/tct-events/tct-asia/sailner-multicolour-material-3d-printing-tct-asia>.
- [2] Yong Lin Kong, Ian A. Tamargo, Hyungsoo Kim, Blake N. Johnson, Maneesh K. Gupta, Tae-Wook Koh, Huai-An Chin, Daniel A. Steingart, Barry P. Rand, and Michael C. McAlpine. 3d printed quantum dot light-emitting diodes. *Nano Letters*, 14(12):7017–7023, 2014.
- [3] Guoxin Fang, Christopher-Denny Matte, Tsz Ho Kwok, and Charlie Wang. Geometry-based direct simulation for multi-material soft robots. In *IEEE International Conference on Robotics and Automation (ICRA)*, pages 1–6, 05 2018.
- [4] Hyunwoo Yuk, Teng Zhang, German Alberto Parada, Xinyue Liu, and Xuanhe Zhao. Skin-inspired hydrogel–elastomer hybrids with robust interfaces and functional microstructures. *Nature Communications*, 7(12028), 2016.
- [5] Christian Duriez, E Coevoet, F Largilliere, T Morales-Bieze, Z Zhang, M Sanz-Lopez, B Carrez, Damien Marchal, Olivier Goury, and J Dequidt. Framework for online simulation of soft robots with optimization-based inverse model. in *IEEE Int. Conf. on Simulation, Modeling, and Programming for Autonomous Robots*, pages 111–118, 12 2016.
- [6] Jonathan Hiller and Hod Lipson. Automatic design and manufacture of soft robots. *IEEE Transactions on Robotics*, 28:457–466, 2012.
- [7] Robert Katzschmann, Andrew D. Marchese, and Daniela Rus. Autonomous object manipulation using a soft planar grasping manipulator. *Soft Robotics*, 2:155–164, 2015.

-
- [8] Andrew D. Marchese, Robert Katzschmann, and Daniela Rus. Whole arm planning for a soft and highly compliant 2d robotic manipulator. *in IEEE Int. Conf. on Intelligent Robots and Systems*, pages 554–560, 2014.
- [9] Mariangela Manti, Taimoor Hassan, Giovanni Passeti, D’Elia Nicolo, Cecilia Laschi, and Matteo Cianchetti. A bioinspired soft robotic gripper for adaptable and effective grasping. *Soft Robotics*, 2(3), 08 2015.
- [10] Hong Kai Yap, Hui Yong Ng, and Raye Chen-Hua Yeow. High-force soft printable pneumatics for soft robotic applications. *Soft Robotics*, 3(3):144–158, 2016.
- [11] Melina Skouras, Bernhard Thomaszewski, Stelian Coros, Bernd Bickel, and Markus Gross. Computational design of actuated deformable characters. *ACM Transactions on Graphics*, 32(4), 2013.
- [12] Nicholas Bartlett, Michael Tolley, Johannes Overvelde, James Weaver, Bobak Mosadegh, Katia Bertoldi, George M Whitesides, and Robert Wood. A 3d-printed, functionally graded soft robot powered by combustion. *Science*, 349:161–5, 2015.
- [13] J.-P. Kruth, M.C. Leu, and T. Nakagawa. Progress in additive manufacturing and rapid prototyping. *CIRP Annals*, 47(2):525 – 540, 1998.
- [14] D.T Pham and R.S Gault. A comparison of rapid prototyping technologies. *International Journal of Machine Tools and Manufacture*, 38(10):1257 – 1287, 1998.
- [15] Sitthi-Amorn Pitchaya, Javier E. Ramos, Yuwang Wangy, Joyce Kwan, Justin Lan, Wenshou Wang, and Wojciech Matusik. Multifab: A machine vision assisted platform for multi-material 3D printing. *ACM Trans. Graph.*, 34(4):129:1–129:11, 2015.
- [16] CHRISTIAN Groth, NEAL D Kravitz, PERRY E Jones, JOHN W Graham, and W RONALD Redmond. Three-dimensional printing technology. *J Clin Orthod*, 48(8):475–85, 2014.

-
- [17] Asim Inamdar, Marco Magana, Frank Medina, Yinko Grajeda, and Ryan Wicker. Development of an automated multiple material stereolithography machine. In *Annual Solid Freeform Fabrication Symposium*, pages 624–635, Austin, TX, 2006.
- [18] Chi Zhou, Yong Chen, Zhigang Yang, and Behrokh Khoshnevis. Digital material fabrication using mask-image-projection-based stereolithography. *Rapid Prototyping Journal*, 19(3):153–165, 2013.
- [19] Jae-Won Choi, Ho-Chan Kim, and Ryan Wicker. Multi-material stereolithography. *Journal of Materials Processing Technology*, 211(3):318 – 328, 2011.
- [20] Jonathan Hiller and Hod Lipson. Dynamic simulation of soft multimaterial 3D-printed objects. *Soft Robotics*, 1(1):88–101, 2014.
- [21] Nick Cheney, Robert MacCurdy, Jeff Clune, and Hod Lipson. Unshackling evolution: evolving soft robots with multiple materials and a powerful generative encoding. In *15th Genetic and Evolutionary Computation Conference*, pages 167–174, 07 2013.
- [22] François Faure, Christian Duriez, Hervé Delingette, Jérémie Allard, Benjamin Gilles, Stéphanie Marchesseau, Hugo Talbot, Hadrien Courtecuisse, Guillaume Bousquet, Igor Peterlik, and Stéphane Cotin. *SOFA: A Multi-Model Framework for Interactive Physical Simulation*, volume 11, pages 283–321. Springer, 06 2012.
- [23] Ramses V. Martinez, Jamie L. Branch, Carina R. Fish, Lihua Jin, Robert F. Shepherd, Rui M. D. Nunes, Zhigang Suo, and George M. Whitesides. Robotic tentacles with three-dimensional mobility based on flexible elastomers. *Advanced Materials*, 25(2):205–212, 2013.
- [24] Andrew A. Stanley and Allison M. Okamura. Deformable model-based methods for shape control of a haptic jamming surface. *IEEE Transactions on Visualization and Computer Graphics*, 23(2):1029–1041, 02 2016.
- [25] Sofien Bouaziz, Mario Deuss, Yuliy Schwartzburg, Thibaut Weise, and Mark Pauly. Shape-up: Shaping discrete geometry with projections. *Comput. Graph. Forum*, 31(5):1657–1667, 2012.

-
- [26] Sofien Bouaziz, Sebastian Martin, Tiantian Liu, Ladislav Kavan, and Mark Pauly. Projective dynamics: Fusing constraint projections for fast simulation. *ACM Trans. Graph.*, 33(4):154:1–154:11, July 2014.
- [27] Tsz-Ho Kwok and Yong Chen. GDFE: Geometry-driven finite element for four-dimensional printing. *Journal of Manufacturing Science and Engineering*, 139(11), 07 2017.
- [28] Shuo Jin, Yunbo Zhang, and Charlie C.L. Wang. Deformation with enforced metrics on length, area and volume. *Computer Graphics Forum*, 33(2):429–438, 2014.
- [29] Isaac Chao, Ulrich Pinkall, Patrick Sanan, and Peter Schröder. A simple geometric model for elastic deformations. *ACM Trans. Graph.*, 29(4):38:1–38:6, 07 2010.
- [30] R.M. Mahamood, E.T.A. Member, Dr Mukul Shukla, and Sisa Pityana. Functionally graded material: An overview. *World Congress on Engineering*, 3:2–6, 01 2012.
- [31] Gururaja Udupa, S. Shrikantha Rao, and K.V. Gangadharan. Functionally graded composite materials: An overview. In *International Conference on Advances in Manufacturing and Materials Engineering, ICAMME 2014*, volume 5, pages 1291 – 1299, 2014.
- [32] Neri Oxman, Elizabeth Tsai, and Michal Firstenberg. Digital anisotropy: A variable elasticity rapid prototyping platform. *Virtual and Physical Prototyping*, 7(4):261–274, 2012.
- [33] S. Khalil, J. Nam, and W. Sun. Multi-nozzle deposition for construction of 3D biopolymer tissue scaffolds. *Rapid Prototyping Journal*, 11(1):9–17, 2005.
- [34] Dan Raviv, Wei Zhao, Carrie McKnelly, Athina Papadopoulou, Achuta Kadambi, Boxin Shi, Shai Hirsch, Daniel Dikovsky, Michael Zyracki, Carlos Olguin, Ramesh Raskar, and Skylar Tibbits. Active printed materials for complex self-evolving deformations. *Scientific Reports*, 4(7422), 2014.

-
- [35] Eric Macdonald, Rudy Salas, David Espalin, Mireya Perez, Efrain Aguilera, Dan Muse, and Ryan B. Wicker. 3D printing for the rapid prototyping of structural electronics. *IEEE Access*, 2:234–242, 2014.
- [36] Lael U. Odhner, Leif P. Jentoft, Mark R. Claffee, Nicholas Corson, Yaroslav Tenzer, Raymond R. Ma, Martin Buehler, Robert Kohout, Robert D. Howe, and Aaron M. Dollar. A compliant, underactuated hand for robust manipulation. *The International Journal of Robotics Research*, 33(5):736–752, 2014.
- [37] Raymond R. and Dollar Aaron M. Odhner, Lael U. and Ma. *Experiments in Under-actuated In-Hand Manipulation*, volume 88, pages 27–40. Springer International Publishing, Heidelberg, 2013.
- [38] M. Tavakoli and A. T. de Almeida. Adaptive under-actuated anthropomorphic hand: Isr-softhand. In *IEEE/RSJ International Conference on Intelligent Robots and Systems*, pages 1629–1634, 09 2014.
- [39] Guanyun Wang, Lining Yao, Wen Wang, Jifei Ou, Chin-Yi Cheng, and Hiroshi Ishii. xPrint: A modularized liquid printer for smart materials deposition. In *Proceedings of the CHI Conference on Human Factors in Computing Systems*, pages 5743–5752. ACM, 2016.
- [40] Lawrence E. Murr. Frontiers of 3d printing/additive manufacturing: from human organs to aircraft fabrication. *Journal of Materials Science & Technology*, 32(10):987 – 995, 2016.
- [41] Joseph Prusa. Multi-material prusa i3 mk2, 2017. <https://www.prusaprinters.org/original-prusa-i3-mk2-multi-material-upgrade-release/>.
- [42] Ming C. Leu, Bradley K. Deuser, Lie Tang, Robert G. Landers, Gregory E. Hilmas, and Jeremy L. Watts. Freeze-form extrusion fabrication of functionally graded materials. *CIRP Annals*, 61(1):223 – 226, 2012.
- [43] Yuri Chivel. New approach to multi-material processing in selective laser melting. *Physics Procedia*, 83:891 – 898, 2016.
- [44] Ali Gokhan Demir and Barbara Previtali. Multi-material selective laser melting of Fe/Al-12Si components. *Manufacturing Letters*, 11:8 – 11, 2017.

-
- [45] Reinout Holtrup. XZEED DLP: a multi-material 3D printer using DLP technology. Bachelor thesis, University of Twente, Enschede, Netherlands, 2015.
- [46] Ryan B Wicker, Francisco Medina, and Chris Elkins. Multiple material micro-fabrication: extending stereolithography to tissue engineering and other novel applications. In *Proceedings of 15th Annual Solid Freeform Fabrication Symposium, Austin, TX*, pages 754–64, 2004.
- [47] Mohammad Vaezi, Srisit Chianrabuttra, Brian Mellor, and Shoufeng Yang. Multiple material additive manufacturing—part 1: a review. *Virtual and Physical Prototyping*, 8(1):19–50, 2013.
- [48] Bose Prosenjit, O’Rourke Joseph, Shu Chang, and Wuhrer Stefanie. Isometric morphing of triangular meshes. *The Canadian Conference on Computational Geometry*, 08 2008.
- [49] Pu Huang, Dongping Deng, and Yong Chen. Modeling and fabrication of heterogeneous three-dimensional objects based on additive manufacturing. In *ASME 2013 International Mechanical Engineering Congress and Exposition*, page V02AT02A056, San Diego, California, USA, 2013.
- [50] Formlabs. Form wash time settings, 2018. <https://support.formlabs.com/hc/en-us/articles/115001347744>.
- [51] F.J. Fuchs. 19 - ultrasonic cleaning and washing of surfaces. In Juan A. Gallego-Juárez and Karl F. Graff, editors, *Power Ultrasonics*, pages 577 – 609. Woodhead Publishing, Oxford, 2015.
- [52] Formlabs. Solvent compatibility, 2018. <https://support.formlabs.com/hc/en-us/articles/115000018064>.
- [53] Reprap project. <http://reprap.org/wiki/RepRap>.
- [54] MakerJuice G+. <https://makerjuice.com/>.